Biogeosciences Discuss., 7, 7029–7090, 2010
www.biogeosciences-discuss.net/7/7029/2010/
doi:10.5194/bgd-7-7029-2010

Biogeosciences Discussions

Sensitivity of the marine carbonate cycle to atmospheric CO_2

R. Gangstø[1,2,*], F. Joos[1,3], and M. Gehlen[2]

[1]Climate and Environmental Physics, Physics Institute, University of Bern, Sidlerstrasse 5, 3012 Bern, Switzerland
[2]LSCE/IPSL, Laboratoire des Sciences du Climat et de l'Environnement, CEA-CNRS-UVSQ, UMR 1572, Orme des Merisiers, Bât. 712, CEA/Saclay, 91198 Gif-sur-Yvette Cedex, France
[3]Oeschger Centre for Climate Change Research, University of Bern, Zähringerstrasse 25, 3012 Bern, Switzerland
[*]now at: Federal Office of Meteorology and Climatology, MeteoSwiss, Zurich, Switzerland

Received: 27 August 2010 – Accepted: 1 September 2010 – Published: 20 September 2010

Correspondence to: R. Gangstø (reidun.gangsto@meteoswiss.ch)

Published by Copernicus Publications on behalf of the European Geosciences Union.

Abstract

Ocean acidification might reduce the ability of calcifying plankton to produce and maintain their shells of calcite, or of aragonite, the more soluble form of $CaCO_3$. In addition to possibly large biological impacts, reduced $CaCO_3$ production corresponds to a negative feedback on atmospheric CO_2. In order to explore the sensitivity of the ocean carbon cycle to increasing concentrations of atmospheric CO_2, we use the new biogeochemical Bern3D/PISCES model. The model reproduces the large scale distributions of biogeochemical tracers. With a range of sensitivity studies, we explore the effect of (i) using different parameterizations of $CaCO_3$ production fitted to available laboratory and field experiments, of (ii) letting calcite and aragonite be produced by auto- and heterotrophic plankton groups, and of (iii) using carbon emissions from the range of the most recent IPCC Representative Concentration Pathways (RCP). Under a high-emission scenario, the $CaCO_3$ production of all the model versions decreases from $\sim 1\,Pg\,C\,yr^{-1}$ to between 0.36 and $0.82\,Pg\,C\,yr^{-1}$ by the year 2100. By the year 2500, the ratio of open water $CaCO_3$ dissolution to production stabilizes at a value that is 30–50% higher than at pre-industrial times when carbon emissions are set to zero after 2100. Despite the wide range of parameterizations, model versions and scenarios included in our study, the changes in $CaCO_3$ production and dissolution resulting from ocean acidification provide only a small feedback on atmospheric CO_2 of 1–11 ppm by the year 2100.

1 Introduction

Ocean uptake of atmospheric CO_2 leads to a decrease in carbonate ion concentrations, a reduction in pH, a shoaling of the calcium carbonate ($CaCO_3$) saturation horizons, and a subsequent increase in $CaCO_3$ dissolution. The current rate at which this process, known as ocean acidification, is occurring will likely have large biological consequences for ocean ecosystems within the near future. Past studies reported

BGD
7, 7029–7090, 2010

a decrease in calcification with decreasing saturation state before undersaturation is reached (refer to Fabry et al., 2008, for a synthesis of existing experimental evidence). Calcifying plankton (mainly coccolithophores, foraminiferas, and pteropods; Schiebel, 2002; Kleypas et al., 2006) might be especially vulnerable to the decreasing saturation state as these organisms secrete calcite and aragonite, two important forms of $CaCO_3$, to form their shells. In addition to potentially large impacts on the marine calcifiers, a decrease in $CaCO_3$ production causes a higher ocean uptake of CO_2. The extent of this negative feedback to atmospheric CO_2 and the changes to the $CaCO_3$ cycle depend to a large extent on the relationship between the calcification of plankton and the saturation state of ambient waters, which may be parameterized from laboratory experiments.

The amount of data published about the response of calcifying organisms to increasing CO_2 has augmented over the last few years. Several studies have focused on warm water corals (e.g. Gattuso et al., 1998; Kleypas et al., 1999; Langdon et al., 2003, 2005). Concerning open ocean calcifying organisms, coccolithophores (and especially *Emiliana huxleyi*) have got much attention (Riebesell et al., 2000; Zondervan et al., 2001, 2002; Sciandra et al., 2003; Delille et al., 2005; Langer et al., 2006; Iglesias-Rodriguez et al., 2008; Shi et al., 2009). The number of experiments performed on foraminifera and pteropods is however growing (e.g. Wolf-Gladrow et al., 1999; Bijma et al., 1999; Fabry et al., 2008; Comeau et al., 2009). The results from the laboratory and mesocosm experiments concerning the relationship between calcification and saturation state are not all consistent. Whereas most studies on corals show an overall strong and linear reduction in calcification with decreasing saturation state (Langdon et al., 2005), the typical magnitude, shape and sign of this relationship for pelagic calcifying plankton is still linked to many uncertainties and is likely to vary with plankton species and group (Fabry et al., 2008).

Various model experiments have been performed during the recent years in order to identify future calcification and dissolution rates in addition to feedback effects on atmospheric CO_2 (Heinze et al., 2004; Ridgwell et al., 2007, 2009; Gehlen et al., 2007;

BGD
7, 7029–7090, 2010

Hofmann and Schnellnhuber, 2009). These were generally fitted to experiments done on coccolithophores (mainly *E. huxleyi*) and $CaCO_3$ was on the form of calcite only. For example, Gehlen et al. (2007) used a Michaelis-Menten type of dependency fitting the results from Riebesell et al. (2000), Zondervan et al. (2001, 2002) and Delille et al. (2005). With the exception of the study by Ridgwell et al. (2007), which provided a relatively large CO_2-calcification feedback response to atmospheric CO_2 when simulating continued carbon emissions after the year 2100, all experiments concluded that the CO_2-calcification feedback would be small. It is estimated that the response of *E. huxleyi* to increasing atmospheric CO_2 is quite small compared to other coccolithophore species, foraminifera and corals (Ridgwell et al., 2007). It is thus possible that biogeochemical models that only let $CaCO_3$ production be associated to this species, may underestimate the CO_2-calcification feedback on atmospheric CO_2. Gangstø et al. (2008) extended the study by Gehlen et al. (2007) to include aragonite and, due to limited data on aragonite producing pteropods, they used a dependency equivalent to Gehlen et al. (2007) to project the response of calcite and aragonite production and dissolution to increasing atmospheric CO_2 concentrations. However, CO_2-calcification feedbacks were not calculated for this model version. No study has yet included in a global biogeochemical model the response of calcite produced by zooplankton (corresponding to foraminifers) to increasing levels of atmospheric CO_2.

We are lead to the following questions: How important is the choice of shape of the relationship fitting the response of calcification to changing carbonate chemistry? Would the inclusion of aragonite and calcite produced by zooplankton change the predicted evolution of $CaCO_3$ production and dissolution, as well as the feedbacks on atmospheric CO_2? How fast is the expected reversibility of the ocean chemistry after a CO_2 perturbation? Would this be affected by the future changes in $CaCO_3$ production and dissolution?

The new cost-efficient Bern3D/PISCES model allows us to explore these aspects further. More recent experiments on both coccolithophores (Iglesias-Rodriguez et al., 2008; Shi et al., 2009) and pteropods (Comeau et al., 2009; J. Büdenbender,

BGD
7, 7029–7090, 2010

S. Lischka, and U. Riebesell, personal communication, 2009) permit us to improve previous studies on the response of calcification to increasing levels of atmospheric CO_2. However, due to a still limited quantity of observations available, only "idealized" scenarios may be projected. We have therefore chosen a sensitivity study approach to our work. We split our study into three parts: In the first part we explore the change in calcite production in response to increasing atmospheric CO_2, using different parameterizations of this response. Here, calcite is produced by nanophytoplankton. In the next section we broaden the study to include aragonite and calcite produced by mesozooplankton, investigating changes in production, dissolution and ocean chemistry in addition to quantifying the associated CO_2-$CaCO_3$ production/dissolution feedbacks. Finally we use a range of emission scenarios to study the sensitivity and evaluate the reversibility of the ocean carbonate system to a CO_2 perturbation.

2 The Bern3D/PISCES model

The Bern3D/PISCES model couples the Bern3D cost-efficient, dynamic ocean circulation model (Müller et al., 2006) and the biogeochemical model PISCES. PISCES was developed within the circulation model NEMO/OPA (Aumont and Bopp, 2006; Gehlen et al., 2006, 2007; Gangstø et al., 2008) which has a relatively high resolution in both time and space requiring large computing resources. The low resolution Bern3D/PISCES model facilitates sensitivity analyses, millennial-scale paleoclimatic studies, and multi-scenario analyses.

2.1 The Bern3D dynamical model

The Bern3D model is a global ocean circulation model (Müller et al., 2006) which is based on the 3-D rigid-lid model of Edwards et al. (1998) and Edwards and Marsh (2005). It has a horizontal resolution of 36 × 36 grid boxes and 32 vertical layers with exponentially increasing thickness towards the ocean bottom. The surface layer

BGD
7, 7029–7090, 2010

has a thickness of 39 m, the bottom layer of 397 m. The atmosphere is described by one well mixed box and the formulations of air-sea gas exchange are based on the updated OCMIP-2 protocol (Orr et al. 1999; Najjar and Orr, 1999), and downscaled by 19% as suggested by Müller et al. (2008). The model is forced with seasonal fields for temperature, salinity and wind stress. Sea surface temperatures and salinities are constrained by using restoring and mixed boundary conditions. Restoring boundary conditions force SST and SSS to remain close to modern-day observational values. With mixed boundary conditions we prescribe freshwater fluxes on the ocean surface instead of SSS, allowing circulation-salinity feedbacks to develop upon perturbation of the model state (Bryan, 1986). An additional freshwater flux correction is applied (by removing freshwater from the Atlantic and distributing it in the North Pacific) in order to intensify and deepen the Atlantic meridional overturning circulation (MOC). The model includes an isopycnal diffusion scheme and Gent-McWilliams parameterization for eddy-induced transport (Griffies, 1998). The standard Bern3D model has been tuned towards data-based chlorofluorocarbon and radiocarbon inventories and is able to capture the large-scale ocean circulation, the characteristics of the most important water masses and the large-scale distributions of a range of ventilation timescale tracers (Müller et al., 2006). The Bern3D model has been applied for a wide range of studies (e.g. Müller et al., 2008; Sidall et al., 2007; Ritz et al., 2008; Tschumi et al., 2008; Parekh et al., 2008; Gerber et al., 2009; Gerber and Joos, 2010).

2.2 The PISCES model

PISCES is a global ocean biogeochemical model (Aumont et al., 2003; Aumont and Bopp, 2006; Gehlen et al., 2006) which simulates the biogeochemical cycle of oxygen, carbon and the main nutrients controlling marine biological productivity: nitrate, ammonium, phosphate, silicate and iron. Biological productivity is limited by the external availability of nutrients and light. The model includes two phytoplankton size classes (nanophytoplankton and diatoms) and two zooplankton size classes (microzooplankton and mesozooplankton). The *C/N/P* ratios are assumed constant for all species. For

BGD
7, 7029–7090, 2010

phytoplankton, the prognostic variables are total biomass, iron, chlorophyll and silicon contents. The internal ratios of Fe/C, Chl/C and Si/C are predicted by the model. For zooplankton, the only prognostic variable is total biomass. The bacterial pool is not modeled explicitly. PISCES comprises three non-living compartments for organic carbon: small particulate organic carbon (POC_s), big particulate organic carbon (POC_b) and semi-labile dissolved organic carbon (DOC). The *C/N/P* composition of dissolved and particulate matter is also coupled to Redfield stochiometry, whereas the iron, silicon and calcite pools of the particles are fully simulated and their ratios relative to organic carbon are allowed to vary. The particulate detrital pools (POC_s, POC_b, biogenic silica and calcite) are fuelled by mortality, aggregation from nanophytoplankton and diatoms, fecal pellet production and grazing. The standard version of the model (Aumont and Bopp, 2006) considers $CaCO_3$ in the form of calcite only and assigns calcite production to nanophytoplankton, albeit without dependency of carbonate production on saturation state. The latter was implemented by Gehlen et al. (2007) for the sake of studying the future evolution of the marine carbonate cycle. The version developed for this study distinguishes two mineral phases of $CaCO_3$, aragonite and calcite (Gangstø et al., 2008). Changes in the concentration of $CaCO_3$ in the mineral form l arise from production, *Prod*, dissolution with the dissolution rate, λ, and sinking of $CaCO_3$ particles with sinking speed ω:

$$\frac{d}{dt}\mathrm{CaCO}_{3,\,l} = \mathrm{Prod}_l - \lambda_l \cdot \mathrm{CaCO}_{3,\,l} - \omega \frac{d}{dz}\mathrm{CaCO}_{3,\,l}. \quad (1)$$

We distinguish between dissolution in the open water and from the ocean bottom. Dissolution in open water occurs only in undersaturated water ($\Omega < 1$) and the rate λ is dependent on the saturation state, Ω, with respect to the appropriate mineral phase:

$$\lambda_l = k \cdot (1 - \Omega_l) \quad \text{for } \Omega_l < 1. \quad (2)$$

$CaCO_3$ particles falling on the ocean floor dissolve immediately in the overlying grid cell independent of Ω. Production of $CaCO_3$ assigned to the plankton of type j and of

BGD
7, 7029–7090, 2010

mineral phase I is taken to be proportional to all the loss terms of this plankton type:

$$\text{Prod}_{j,I} = R_{j,I} \cdot \{\text{Loss Terms}\}_j. \quad (3)$$

No production of calcite or aragonite occurs if the water is undersaturated with respect to the appropriate mineral phase. In oversaturated water, the fraction $R_{j,I}$ is not allowed to fall below 0.01 or exceed 0.8. The model simulates dissolved inorganic carbon and total alkalinity. The carbon chemistry follows the OCMIP protocol (http://www.ipsl.jussieu.fr/OCMIP). A detailed description of the model including model equations and parameters can be found as auxiliary material in Aumont and Bopp (2006).

2.2.1 Calcite production by nanophytoplankton

The equations for calcite production by nanophytoplankton in the PISCES model are detailed by Gehlen et al. (2007). The proportion of calcifying phytoplankton is low in oligotrophic regions and calcifiers are often the dominant species when nanophytoplankton blooms. To mimic these conditions, the following parameterization is applied for $R_{\mathrm{P,\,C}}$ (Aumont and Bopp, 2006):

$$R_{\mathrm{P,\,C}} = f_i \cdot L^P_{\mathrm{lim}} \cdot \max\left(0.0001, \frac{T}{2+T}\right) \cdot \max\left(1, \frac{P}{2}\right) \cdot \left(\frac{\mathrm{PIC_C}}{\mathrm{POC}}\right)_i. \quad (4)$$

In this parameterization, f_i is a scaling factor used to tune global calcite production by nanophytoplankton. L denotes limitation by the availability of phosphate, nitrate, ammonium, and iron and is taken to be identical to the nutrient limitation factor for nanophytoplankton growth. T is water temperature in $^\circ$C and P is mass of nanophytoplankton in units of mol C l^{-1}. The last factor in above equations denotes the ratio of inorganic to organic carbon for calcifying nanophytoplankton under optimal condition and as a function of the saturation state. Subscript i refers to different parameterizations of the ratio of particulate inorganic carbon (PIC) to particulate organic carbon (POC), $\mathrm{PIC_C/POC}$, and subscript C to calcite.

BGD
7, 7029–7090, 2010

According to experimental results of the coccolithophore *E. huxleyi* obtained by Riebesell et al. (2000), Zondervan et al. (2001, 2002) and Delille et al. (2005), the calcification rate may be described by a threshold value of the saturation state below which the calcification decreases rapidly. Gehlen et al. (2007) fitted the PIC_C/POC variable to these experimental results. Since then, new experiments with *E. huxleyi* have been performed (Iglesias-Rodriguez et al., 2008; Shi et al., 2009). When considering the calcification rates, these studies show an increase with decreasing saturation state, which is in contrast to previous studies on *E. huxleyi*. However, when looking at the PIC-POC values, the data points from these two studies fit well into the group of the other experimental data (Fig. 1). For all the experimental studies, the PIC-POC ratio decreases with decreasing saturation state; however the data from the most recent studies (black symbols) show a weaker response and may possibly be better described by a linear decrease with decreasing saturation state.

1. Michaelis-Menten type relationship between calcite production and saturation

In previous studies (Gehlen et al., 2007; Gangstø et al., 2008) a Michaelis-Menten approach was adopted for the PIC-POC ratio of calcifying nanophytoplankton, in order to mimic the decreasing calcification with decreasing saturation state (Riebesell et al., 2000; Zondervan et al., 2001, 2002; Delille et al., 2005). The PIC-POC ratio for calcifying nanophytoplankton as a function of saturation state is expressed as:

$$\left(\frac{\mathrm{PIC_C}}{\mathrm{POC}}\right)_{\mathrm{MIC}} = \left(\frac{\mathrm{PIC_C}}{\mathrm{POC}}\right)_{\mathrm{max}} \times \frac{(\Omega_C - 1)}{K_{\mathrm{max}} + (\Omega_C - 1)}, \text{ for } (\Omega_C - 1) > 0. \quad (5)$$

$(\mathrm{PIC_C/POC})_{\mathrm{max}}$ is the maximum ratio reached under optimal growth conditions for calcifying organisms and K_{max} corresponds to a half saturation constant. Ω_C is the saturation state with respect to calcite.

The values $(\mathrm{PIC_C/POC})_{\mathrm{max}}$ and K_{max} were previously set equal to 0.8 and 0.4, respectively (Gehlen et al., 2007; Gangstø et al., 2008). New data published (Iglesias-Rodriguez et al., 2008; Shi et al., 2009) encourage us to make a new fit, termed MIC1,

BGD
7, 7029–7090, 2010

to the data. Only data without severe light limitations and nutrient limitation are considered (Zondervan et al., 2007), thus excluding one of the data sets from Zondervan et al. (2002), in addition to another data set which should be discarded due to large uncertainties (Zondervan et al., 2002). These two data sets were included in the original fit MIC2. The new fit MIC1 provides an upper limit of the PIC-POC value for calcifying organisms equal to 1.04, whereas K_{max} becomes 1.11. The PIC_C/POC ratio is shifted upwards for high saturation state values for the new fit MIC1 compared to the fit MIC2 (Fig. 1). We refer to simulations with the new parameterization by the term "CALMIC1", to those with the original fit by "CALMIC2" (Table 1).

2. Linear relationships between calcite production and saturation

As the quantity of experiments performed on pelagic plankton is not yet massive, we may question the validity of using a Michaelis-Menten type correlation, and wonder how the use of a linear relationship between $CaCO_3$ production and saturation state would influence projected calcification. No $CaCO_3$ production is allowed in undersaturated water. In parameterization LIN1, (PIC_C/POC) and thus production is forced to go through zero for Ω_C equal one:

$$\left(\frac{PIC_C}{POC}\right)_{LIN1} = \text{ppcal} \cdot (\Omega_C - 1), \text{ for } (\Omega_C - 1) > 0, \quad (6)$$

with the slope ppcal equal to 0.19.

In parameterization LIN2, data points are fitted with no forcing (the production is still set to 0 when the saturation state becomes smaller than 1):

$$\left(\frac{PIC_C}{POC}\right)_{LIN2} = \text{ppcal2} + \text{ppcal3} \cdot (\Omega_C - 1), \text{ for } (\Omega_C - 1) > 0. \quad (7)$$

The offset ppcal2 is 0.55 and the slope ppcal3 is with 0.06 more than three times smaller than in LIN1 (Fig. 1). We expect thus a stronger response in calcite production for LIN1 than for the other parameterizations. We refer to the linear parameterization

BGD
7, 7029–7090, 2010

forced through zero (Eq. 6) by "CALLIN1" and to the unconstrained linear fit (Eq. 7) by "CALLIN2" (Table 1).

2.2.2 Aragonite production by mesozooplankton

The equations for aragonite production and dissolution are specified in Gangstø et al. (2008). The production is assigned to mesozooplankton as a function of saturation state of seawater with respect to aragonite. Due to the limited observations available, the modeled dependency of the calcification on saturation state was done in an equivalent way as for calcite following a Michaelis Menten curve.

Recently, new data has become available. Comeau et al. (2009), who studied the response in calcification of the pteropod *Limacina helicina* to decreasing saturation states, reports a decrease in aragonite production of 28% with a reduction in saturation state from 1.9 to 1.0 (CO_2 increased from 350 to 760 uatm). No PIC and POC values were given in their study. Another study on *L. helicina* performed in Kongsfjorden provided PIC and POC values (J. Büdenbender, S. Lischka, and U. Riebesell, personal communication, 2009). A linear relationship is developed from the two data sets. We assume that the maximum PIC-POC value of the second study of about 0.106 corresponds to conditions with Ω_A equal 1.9 and that PIC_A/POC is 28% lower for saturation ($\Omega_A = 1$) to obtain a value for the future saturation conditions. This yields:

$$\left(\frac{\mathrm{PIC_A}}{\mathrm{POC}}\right)_{\mathrm{M}} = \mathrm{pparag} + \mathrm{pparag2} \cdot (\Omega_A - 1), \text{ for } (\Omega_A - 1) > 0, \quad (8)$$

where the offset pparag equals 0.076 and the slope pparag2 is 0.033. The PIC-POC ratio is multiplied with mesozooplankton biomass, M, a scaling factor $f_{\mathrm{M,\,A}}$, and the sum of the loss terms for mesozooplankton to yield aragonite production. The factor $R_{\mathrm{M,\,A}}$ for aragonite production by mesozooplankton becomes:

$$R_{\mathrm{M,\,A}} = f_{\mathrm{M,\,A}} \cdot \mathrm{M} \cdot \left(\frac{\mathrm{PIC_A}}{\mathrm{POC}}\right)_{\mathrm{M}}. \quad (9)$$

BGD
7, 7029–7090, 2010

In contrast to the factor R, for nanophytoplankton, $R_{M,\,A}$ does not depend on temperature and nutrient limitation. We refer to the simulation including the aragonite parameterization (Eq. 9) and the new Michaelis-Menten parameterization for calcite (Eq. 5) as "CALARAG" (Table 1).

2.2.3 Calcite production by mesozooplankton

Foraminifers are, in addition to coccolithophores, major calcite producers in the pelagic ocean. They may account for between 32 and 80% of the $CaCO_3$ that accumulates on the sea floor (Schiebel, 2002). They are an important link to the upper trophic levels (e.g. Legendre and Le Févre, 1995; Rowe et al., 2008). Studies of foraminifera show reduced calcification in response to ocean acidification (e.g. Wolf-Gladrow et al., 1999; Bijma et al., 1999; Lombard et al., 2009). Most of these studies include changes in shell weight only. The shell mass was reported to decrease by 4–8% for a doubling of atmospheric CO_2 (Spero et al., 1997; Bijma et al., 1999). Moy et al. (2009) suggest that a decrease in shell weight of 30–35% may have taken place since pre-industrial times (thus within less than a doubling of atmospheric CO_2). Dissard et al. (2009) confirms the correlation between change in carbonate ions and change in shell weights. Lombard et al. (2009) project a decrease in shell weight of between 20 and 27% within the end of the century. The decrease in shell weight is in some studies reported to be non-linear (Bijma et al., 2002; Kuroyanagi et al., 2009), and in another study linear (Lombard et al., 2009). When it comes to changes in calcification rates of foraminifers, we are only aware of the data by Lombard et al. (2009). They suggest a reduction in calcification rates of between 6 and 13% by the end of this century compared to present day conditions, and these data indicate a linear shape of the response in calcification to increasing atmospheric CO_2.

A linear relationship to simulate the response in calcite production by foraminifera to decreasing saturation state is used here. We have chosen to use the unforced linear dependency on saturation state for the corresponding PIC/POC variable:

BGD
7, 7029–7090, 2010

$$\left(\frac{\mathrm{PIC_C}}{\mathrm{POC}}\right)_{\mathrm{M}} = \mathrm{ppcal2} + \mathrm{ppcal3} \cdot (\Omega_C - 1) \text{ for } (\Omega_C - 1) > 0, \quad (10)$$

and to describe the fraction $R_{\mathrm{M,\,C}}$ for calcite production by mesozooplankton:

$$R_{\mathrm{M,\,C}} = f_{\mathrm{M,\,C}} \cdot \mathrm{M} \cdot \left(\frac{\mathrm{PI_C}}{\mathrm{POC}}\right)_{\mathrm{M}}, \quad (11)$$

where $f_{\mathrm{M,\,C}}$ is again a tuning factor. The parameter ppcal2 is set to 0.55 and ppcal3 to 0.06. We refer to the simulation including the aragonite parameterization (Eq. 5), the new Michaelis-Menten parameterization for calcite (Eq. 1), and the calcite parameterization from Eqs. (10) and (11) as "CAL2ARAG".

3 Model setup and simulations

In the current study we use the parameter values for the Bern3D model as given by Müller et al. (2006), with a few exceptions. The diapycnal diffusivity has been increased from $1 \times 10^{-5}\,\mathrm{m\,s^{-2}}$ to $5 \times 10^{-5}\,\mathrm{m\,s^{-2}}$ and the Atlantic-to-Pacific freshwater flux correction was set equal to 0.2 Sv in order to strengthen the circulation fields and subsequently improve the oxygen and nutrients fields of the biogeochemical model. The time step used for the Bern3D model is reduced by a factor of 2 compared to the standard version (Müller el al., 2006), with the PISCES component called every $\sim$2 h in order to assure numerical stability.

The model alkalinity field was initialized with a global mean alkalinity value of 2410 mol/m^3, which lies between the global average from GLODAP (Key et al., 2004) and the one from Goyet et al. (2000). In the NEMO/PISCES model, half of the fraction of calcite production that is linked to loss of nanophytoplankton by grazing is assumed to be dissolved in the guts of zooplankton; only the remaining half affects alkalinity in open water and is added to the $CaCO_3$ pool (Aumont and Bopp, 2006). In this study,

BGD
7, 7029–7090, 2010

the percentage of $CaCO_3$ that interacts with the alkalinity pool is increased from 0.5 to 0.85, which slightly improves the alkalinity fields. Nitrogen fixation and denitrification as well as river input and silicate deposition from dust were all set to 0 in the present study. In order to improve low oxygen values at depth and low surface concentrations of nutrients resulting from differences in circulation strength between the two dynamical models, the sinking speed of the largest class of particulate organic carbonate (POC_b) was reduced to a constant value of $60\,m\,d^{-1}$. Total pre-industrial $CaCO_3$ production is tuned in all setups to about $1.0\,Pg\,C\,yr^{-1}$ by adjusting the scaling factors in Eqs. (4) and (11).

The physical Bern3D model was first integrated over 10 000 years using restoring boundary conditions. Next, air-sea freshwater fluxes were diagnosed and averaged over the last 1000 years to provide mixed boundary conditions. The model was then switched to mixed boundary conditions, and an additional freshwater flux from the Atlantic to the Pacific was included. The model was further run for 5000 years. Finally, the PISCES model was added and the Bern3D/PISCES model was integrated over 3000 years with atmospheric CO_2 concentrations kept constant at 278 ppm (parts per million). Annual means were calculated and are used in the entire study.

Nine model versions are run to explore the projected changes in calcification to increasing atmospheric CO_2 concentrations, six with and three, termed NODEPC, NODEPCA, NODEPC2A, without a dependency of calcification on saturation state (Table 1). Atmospheric CO_2 is prescribed for the period from 1766–2006. From 2007–2100, projected CO_2 emissions of the IPCC scenarios RCP8.5 (referred to as High) and RCP6 (Medium) are used (Van Vuren et al., 2008; Strassmann et al., 2009) in addition to a scenario with zero carbon emissions (Low). Most of the model versions are run with the High scenario only, whereas multi-scenario runs are performed with the CALARAG and NODEPCA versions (Table 1). From year 2100 to year 2500 the CO_2 emissions are set to 0. All scenario runs are accompanied with corresponding control runs with constant pre-industrial CO_2 concentrations.

BGD
7, 7029–7090, 2010

4 Results

4.1 Model evaluation/pre-industrial state

4.1.1 Circulation and water masses

Maximum overturning reaches 23 Sv (1 Sv = 10^6 m^3 s^{-1}) at around 45° N in the North Atlantic, with a southward transport out of the Atlantic between 1000 and 2000 m depth of about 16 Sv (Fig. 2). This is comparable to the estimates of Talley et al. (2003) of maximum overturning and southward transport equal to 18 Sv for most latitudes. The modeled overturning is larger than in earlier model versions (Müller et al., 2005) where a lower diapycnal diffusivity has been applied. North Atlantic Deep Water (NADW) is now propagating somewhat too deep as evidenced by the comparison between modeled and data-based radiocarbon fields from GLODAP (not shown). A weak modeled overturning cell in the deepest part of the Atlantic corresponds to AABW. The value of the transport from the AABW is lower than estimates, which suggests a transport up to 8.5 Sv (Talley et al., 2003). In the South Pacific, the northward flow of AABW takes place below 2000 m and maximum deep overturning is 14 Sv, comparable to the estimate by Talley et al. (2003) of 13 Sv. Deep equatorial upwelling in the Pacific is with about 9 Sv likely too much and results in some nutrient trapping in the thermocline of the equatorial Pacific (not shown). The formation of North Pacific Intermediate Water (NPIW) is rather strong compared to observations (Talley et al., 2003), and propagates too deep. Although most of the Pacific deepwater is supposed to flow southwards again at intermediate depths, too high radiocarbon values at the surface of the North Pacific compared to observations may indicate too little upwelling of old water masses here. Deep convection occurs mainly in the North Atlantic south of Greenland and in the Ross and Weddell Sea next to Antarctica. Compared to the standard Bern3D model as used in earlier studies, the Bern3D/PISCES simulates more overturning and younger water masses. As far as the marine biological cycle is concerned, we expect

BGD
7, 7029–7090, 2010

too much biological production and too much nutrient trapping in the equatorial Pacific due to upwelling.

4.1.2 $CaCO_3$ production

The spatial pattern of modeled $CaCO_3$ production (Fig. 3) shows the major large-scale features of the observations (Iglesias-Rodriguez et al., 2002a; Balch et al., 2007). Values are low in the ocean gyres and high in the North Atlantic, North Pacific, and Southern Ocean, as well as in the near coastal upwelling zones in the eastern Pacific and eastern South Atlantic. The modeled production reaches about 12 $gC\,m^{-2}\,yr^{-1}$ in the areas with maximum concentrations of nanophytoplankton. The model seems to overestimate the calcification in the lower latitudes compared to the satellite-based distribution patterns of coccolithophorid blooms (Iglesias-Rodriguez et al., 2002a) and surface calcification (Balch et al., 2007).

In regions away from the coast, differences in modeled $CaCO_3$ production are relative small between the different model versions (Fig. 3). In other words, $CaCO_3$ production by nanophytoplankton and by mesozooplankton has a similar spatial pattern. This reflects the dependency of mesozooplankton on the availability of nanophytoplankton as a source of food. Mesozooplankton graze on nanophytoplankton, in addition to grazing on diatoms, microzooplankton and POC. In near-coastal areas, the $CaCO_3$ production is, however, substantially higher in the versions CALARAG and CAL2ARAG where 1/3 and 2/3 of the production are related to mesozooplankton (Fig. 3). Zonally-averaged production is higher in the Southern Ocean ($< 50^{\circ}$ S) and for the maximum south of the equator for the version with mesozooplankton calcification (CALARAG, CAL2ARAG) than for the versions with $CaCO_3$ production by nanophytoplankton only (Fig. 4a). This reflects the relatively higher abundance of mesozooplankton in these productive regions. The model versions with no dependency of $CaCO_3$ production on saturation state broadly follow similar zonal patterns.

Observations and estimates of pteropod and foraminifera calcification are scarce. Most of the aragonite production occurs in subpolar and polar areas (Lalli and Gilmer,

BGD
7, 7029–7090, 2010

1989). Sediment trap studies have shown that in the Southern Ocean, south of the Polar Front, pteropods are the major source of the carbonate flux (>50%) to the depth (Hunt et al., 2008). In the Sub-Antarctic Zone, tests from coccolithophores and foraminifers dominate the flux (Honjo et al., 2000; Honjo, 2004). The model versions with aragonite both provide quite high $CaCO_3$ production rates in polar and subpolar areas, coherent with literature reporting that aragonite shells of pteropods are especially abundant here (e.g. Collier et al., 2000; Honjo et al., 2000; Urban-Rich, 2001; Accornero et al., 2003). However, an even higher aragonite production is simulated in lower latitudes. While studies report that pteropods are also significant contributors to the $CaCO_3$ flux in low latitudes, such as in the Indian Ocean (Panchang et al., 2007) and the Equatorial Atlantic (Volbers et al., 2001), the highest biomass of pteropods is expected to be found in cold, high-latitude waters (Lalli and Gilmer, 1989). This may indicate an overestimation of aragonite production in low latitudes by the Bern3D/PISCES model. Since aragonite production is linked to the modeled mesozooplankton distribution, a bias in the latter could explain the latitudinal trend. A comparison between a compilation of observations by Buitenhuis et al. (2006) and model output (not shown), demonstrates that the overall spatial variability in mesozooplankton distribution is fairly well reproduced by the models. This leaves us with the suggestion that the latitudinal trend with higher average rates of aragonite production occurring at low latitudes might reflect a missing temperature effect on aragonite production and that mesozooplankton is represented by one single group only.

$CaCO_3$ production is simulated down to a depth of ~500 m with little differences in basin-averaged production profiles between the different model versions (Fig. 5d). Most of the production is simulated above 200 m, consistent with the fact that both coccolithophorids (nanophytoplankton) and pteropods (mesozooplankton) are mostly found in near-surface water in the upper 200 m, while a few pteropod species are restricted to deeper waters.

In conclusion, $CaCO_3$ production appears to be reasonably represented in the Bern3D/PISCES model when compared with available observation-based estimates

BGD
7, 7029–7090, 2010

and their uncertainty. Aragonite production is likely overestimated in low and mid-latitude regions as production is linked to mesozooplankton abundance without considering that many aragonite producing species are found predominantly in cold, high-latitude waters.

4.1.3 Alkalinity and DIC

The observed spatial patterns of DIC and alkalinity in the surface ocean are well matched by the model (Figs. 4 and 6). The Bern3D/PISCES reproduces the high alkalinity values in the north and south Atlantic and the high DIC concentrations in the Southern Ocean. However, the surface alkalinity and DIC concentrations are on average lower than observed. This suggests that $CaCO_3$ production, tuned to 1.0 Pg C yr^{-1}, is too high relative to the alkalinity supply from the thermocline. DIC and alkalinity are slightly higher in the versions including aragonite production and dissolution. This is due to the 50% higher solubility of aragonite compared to calcite, which increases shallow dissolution and thus the alkalinity and DIC concentrations at the surface and in the upper part of the water column. Consequently, including aragonite in the model improves the simulated concentrations of surface alkalinity and DIC.

At depth, the model generally reproduces observation-based alkalinity and DIC patterns (Fig. 5a and b). Existing mismatches can be explained by deficiencies in the simulated ocean circulation. DIC and alkalinity increase along the deep ocean transport path, due to the water column remineralization of organic carbon and $CaCO_3$. Modeled DIC concentrations in most of the Atlantic are low compared to observations and for all model versions. This is likely related to the large formation rate and deep penetration of relatively carbon poor NADW. High DIC and alkalinity concentrations are found in the very deep Atlantic, which is partly linked to the too weak AABW spreading in the Atlantic. The substantial trapping of alkalinity in the deep Atlantic contributes to the low alkalinity concentrations modeled in the deep Pacific as the total ocean alkalinity inventory is fixed. Modeled alkalinity and DIC are higher than observations in the

BGD
7, 7029–7090, 2010

intermediate (~ 1000–2000 m) Pacific as expected from the modeled large equatorial upwelling.

The alkalinity and DIC concentrations at depth are somewhat improved in the versions including aragonite, due to the rearranging of DIC and alkalinity concentrations in the water column caused by shallow water aragonite dissolution. An exception is the simulated high alkalinity and DIC concentrations at intermediate depths of the Indian Ocean, which may be related to the peak of aragonite dissolution in this area (Fig. 5). The differences between the model versions with calcite only and the model versions including aragonite may further be seen in the Taylor diagram (Fig. 7), where modeled alkalinity and DIC are compared to pre-industrial values from the Global Ocean Data Analysis Project (GLODAP) (Key et al., 2004). The correlation coefficient r between modeled and data-based alkalinity is ~ 0.8 for the versions without aragonite, and ~ 0.7 for the versions including aragonite. For DIC, the correlation coefficient is higher than 0.9 for all versions and independent of the form of $CaCO_3$, whereas the standard deviation becomes closer to unity when aragonite is included. To conclude, the observed alkalinity and DIC concentrations are fairly well represented by the model, except for some discrepancies in the Atlantic and Pacific mainly related to deficiencies in modeled circulation. Including aragonite tends to slightly improve the distribution of alkalinity and DIC both at the surface and in the water column.

4.1.4 Saturation state

Modeled surface CO_3^{2-} concentrations and aragonite saturation state compare well with observations (Fig. 6e and f). The modeled surface aragonite saturation state is on average slightly too high (Fig. 4b). At depth, the observed values of CO_3^{2-} and aragonite saturation state are relatively well represented in the Southern and Indian Ocean (Figs. 5c and 8), with aragonite saturation horizons around the depth of 1000 m (Fig. 8). Mismatches between model results and observations in the Atlantic and Pacific (Figs. 5c and 8) may be linked to deficiencies in the modeled DIC and alkalinity fields. The concentration of CO_3^{2-} is roughly proportional to the difference between

BGD
7, 7029–7090, 2010

alkalinity and DIC, so that high alkalinity or low DIC concentrations would generally affect the water masses in direction of increased saturation state. As a consequence, CO_3^{2-} is too high in most of the Atlantic, resulting in too deep calcite and aragonite saturation horizons compared to observations (Fig. 5c). In the Pacific, modeled CO_3^{2-} concentrations are too low at depth, which results in a too shallow saturation horizon for calcite (Fig. 5c). Finally, in the upper 1000 m of the Pacific, the modeled CO_3^{2-} concentrations are too high and the aragonite saturation horizon too deep as DIC concentrations are underestimated (Figs. 5b and 8). Despite some discrepancies, the Taylor diagram (Fig. 7) shows a correlation coefficient of 0.95 for all versions and a relative standard deviation just above unity, when modeled Ω_A is compared to GLODAP observations. This indicates an overall good representation of the aragonite saturation state in the Bern3D/PISCES. This is particularly important in the context of the current study where $CaCO_3$ production and dissolution is described as a function of saturation.

4.1.5 Global carbonate budgets

Next, the global pre-industrial $CaCO_3$ production, export and dissolution fluxes are discussed in the context of observation-based estimates and compared with those from the NEMO/PISCES model (Tables 1 and 2) (Gehlen et al., 2007; Gangstø et al., 2008). Total $CaCO_3$ production was tuned to $\sim 1\,Pg\,C\,yr^{-1}$ for all versions and fits well within the range of estimates (Iglesias-Rodriguez et al., 2002b; Lee, 2001; Jin et al., 2006; Berelson et al., 2007; Balch et al., 2007). The modeled $CaCO_3$ export at 100 m (0.8 to 0.89 PgC/yr) is smaller than the net production, because $CaCO_3$ is also produced below 100 m (Fig. 5d). Model export matches well the estimate by Berelson et al. (2007), but is higher than proposed by Sarmiento et al. (2002). One third of the $CaCO_3$ production was assigned to aragonite in the model versions CALARAG and CAL2ARAG following Gangstø et al. (2008). The percentage is in the upper range of most estimates and was chosen to permit the identification of an approximate upper

BGD
7, 7029–7090, 2010

limit to which aragonite may contribute to shallow depth $CaCO_3$ dissolution. Pelagic aragonite production is often supposed to contribute 10% to the total pelagic $CaCO_3$ production, based on Fabry (1990). However, estimates of aragonite production and fluxes in the pelagic ocean are scarce and cover a large range, extending from 10 to 50% of the total global $CaCO_3$ flux (Berner, 1977; Berger, 1978; Berner and Honjo, 1981; Fabry and Deuser, 1991). An estimate based upon geochemical tracer inversion (Munhoven, 2007) supports our aragonite production fraction of one third.

The modeled $CaCO_3$ dissolution rates within the water column are within the range of estimates for all model versions. The total pelagic $CaCO_3$ dissolution is substantially lower in calcite only versions (CALMIC1 and CALMIC2; $\sim 0.4\,Pg\,C\,yr^{-1}$) than in those with aragonite (CALARAG and CAL2ARAG ; $\sim 0.6\,Pg\,C\,yr^{-1}$). This is related to the higher solubility of aragonite compared to calcite. Including aragonite in the model yields a substantial $CaCO_3$ dissolution in the upper part of the water column compared to the version without aragonite (Fig. 5e, Table 2). This increased shallow water $CaCO_3$ dissolution in CALARAG, compared to CALMIC1 and CALMIC2, matches better with observation-based estimates (Feely et al., 2004; Milliman and Droxler, 1996) and confirms the results found by Gangstø et al. (2008). It also supports the hypothesis that the estimated loss of $CaCO_3$ or excess of alkalinity in the upper part of the water column may be at least partly attributed to aragonite dissolution (Milliman and Droxler, 1996; Berelson et al., 2007).

Total $CaCO_3$ production and export production are higher in the Bern3D/PISCES model than in NEMO/PISCES. In NEMO/PISCES, production is with 0.79 to 0.87 PgC/yr close to the lower end of the estimated range (Table 2). Recall that global production is tuned by adjusting a scaling factor. Open water calcite dissolution corresponds to only 38 to 40% of production in the calcite-only version of the Bern3D model compared to 61% in the NEMO/PISCES calcite-only version. This difference is mainly related to the generally high modeled concentrations of CO_3^{2-} in the Bern3D/PISCES versions especially at depth in the Southern and Indian Ocean (Fig. 5c, blue dashed line). The resulting calcite saturation horizons in these basins are deeper (Fig. 5c),

BGD
7, 7029–7090, 2010

leading to lower calcite dissolution in the water column in the Bern3D/PISCES model than in the NEMO/PISCES model.

In summary, the global $CaCO_3$ production, export and dissolution fluxes in the Bern3D/PISCES model are comparable to observation-based estimates. The representation of the $CaCO_3$ cycle in the cost-efficient Bern3D/PISCES is comparable to that in NEMO/PISCES, despite some differences between the two models in the saturation state and the global $CaCO_3$ production.

4.2 Future projections: sensitivity to parameterizations, feedbacks and reversibility

4.2.1 Atmospheric CO_2 and saturation state

Next, we will discuss the projected anthropogenic perturbation in the $CaCO_3$ cycle and the evolution of underlying drivers for carbon emission commitment scenarios (e.g. Frölicher and Joos, 2010). Carbon emissions are prescribed up to 2100 according to one of the RCP scenarios and then hypothetically (and unrealistically) set to zero to study the long-term impacts of 21st century emissions on the $CaCO_3$ cycle and CO_2. We will first discuss results for the high-emission, no climate-policy intervention scenario, before discussing the range of scenarios in Sect. 4.2.5. Note that global warming is not modeled here and production of organic material remains constant throughout the simulation. The changes in $CaCO_3$ production and dissolution are thus only forced by changes in the saturation state with respect to $CaCO_3$. The evolution of $CaCO_3$ production is therefore closely linked to the evolution of the saturation state in the surface ocean (Figs. 9b and 10), which itself closely follows atmospheric CO_2 (Fig. 13). The evolution of open water $CaCO_3$ dissolution is influenced by the extent of undersaturated water (Fig. 11) and the degree of undersaturation.

Differences in projected changes in CO_2, in surface saturation with respect to calcite (Ω_C) or aragonite (Ω_A) and in the volume of undersaturated water are relatively small between the different model versions (Figs. 9, 10, and 11). This implies that differences

BGD
7, 7029–7090, 2010

in $CaCO_3$ production and dissolution are directly related to differences in the parameterization of $CaCO_3$ production. Atmospheric CO_2 increases to almost 1000 ppm by 2100 for the High scenario. Afterwards, CO_2 decreases only slowly to about 600 ppm by 2500 AD, even though emissions are zero after 2100. Ω_C decreases from about 5.2 to 2.2 and Ω_A from about 3.4 to about 1.4 by the year 2100 and for all versions (Fig. 9b). Saturation increases again afterwards at the surface. Regionally, the largest decrease in saturation are found in the tropics, whereas surface waters in high-latitude become undersaturated with respect to aragonite over the course of this century and remain undersaturated by 2500 under the High scenario (Fig. 10). Undersaturation with respect to aragonite is imminent in the Arctic and becomes also widespread in the Southern Ocean. The evolution of the surface ocean aragonite saturation state projected by model versions CALARAG and NODEPCA (Fig. 10) is close to identical up to the year 2100 and differences are small after 2100. In other words, the overall effect from the decreasing calcification on the saturation state is small.

Following Steinacher et al. (2009) and Frölicher and Joos (2010), we distinguish different classes of saturation with respect to aragonite and compute global changes in the volume occupied by undersaturated and oversaturated water masses as an indicator of whole ocean acidification (Fig. 11). The volume of water oversaturated with respect to aragonite decreases from about 60% to only 15% of the ocean volume until 2200. Correspondingly, the volume fraction of undersaturated water, where $CaCO_3$ particles dissolve, increases. Saturation changes long after emissions have been stopped as anthropogenic carbon continues to invade the slowly ventilated deep ocean. Water that is more than three times supersaturated disappears in the next decades and remains absent until the year 2400 for the High case. This illustrates the long-lasting impacts of anthropogenic carbon emissions. Our results are consistent with simulations with the comprehensive NCAR climate-carbon cycle model and we refer to the literature for a further discussion on changes in the saturation state and the reversibility of the impacts of 21st century emissions on the carbon cycle and climate (Frölicher and Joos, 2010; Steinacher et al., 2009).

BGD
7, 7029–7090, 2010

4.2.2 $CaCO_3$ production and dissolution

The $CaCO_3$ production changes in response to changes in surface saturation. In most of the calcite-only version the production decreases to between 0.79 and 0.82 Pg C yr^{-1} until 2100 and for the High case (Fig. 9c). This corresponds to a 20–34% reduction relative to pre-industrial values. The exception is version CALLIN1 with a reduction of 66%. In this version the rain ratio is forced to zero for Ω_C approaching one and the production depends particularly sensitively on saturation. After 2100, the $CaCO_3$ production increases again, following the increase in saturation state and the decrease in CO_2. By the end of the scenario, at the year 2500, the production in the CALLIN1 version with the most sensitive parameterization has increased to about 0.6 Pg C yr^{-1}, compared to $\sim$0.9 Pg C yr^{-1} for the other 3 calcite-only versions (Fig. 9c). Hence, with the exception of the more extreme linear parameterization, the different calcite parameterizations shown in Fig. 1, whether linear or functions of a Michaelis-Menten curve, provide similar responses of the calcite production to the simulated perturbation in the saturation state.

The two versions including aragonite, CALARAG and CAL2ARAG, generally yield a larger decrease in $CaCO_3$ production than the versions with calcite only (Fig. 9c). The total $CaCO_3$ production (calcite and aragonite) decreases by 35 and 31% within the year 2100 for the versions CALARAG and CAL2ARAG, respectively (Table 3). By the year 2500, the production has reached 0.80 and 0.78 Pg C yr^{-1}, respectively, corresponding to a 19 and 18% decrease compared to pre-industrial times. The larger reduction in $CaCO_3$ production of the versions including aragonite is caused by the higher solubility of aragonite particles compared to calcite particles. The aragonite saturation state is lower than the calcite saturation state already at pre-industrial times (Fig. 9b) and it decreases to even lower values with increasing atmospheric CO_2.

The magnitude of $CaCO_3$ dissolution in the open water column (Fig. 9d) depends (i) on the amount of $CaCO_3$ produced (Fig. 9c), and (ii) on the saturation state with respect to $CaCO_3$ in the thermocline and deep ocean (Fig. 11). The relative importance

BGD
7, 7029–7090, 2010

of the two factors is quantified with the help of simulations that do not include a dependency of the $CaCO_3$ production on the saturation state. In these simulations, labeled "NODEP", production remains constant and changes in dissolution are entirely driven by changes in the dissolution rate (Eq. 2).

Global $CaCO_3$ dissolution in the open water increases to reach a plateau after 2200 in the NODEP cases for the High scenario. The evolution in dissolution roughly parallels the increase in the volume of undersaturated water (Fig. 11). The volume of undersaturated water increases for another century after emissions have been stopped in 2100 as the ocean continues to take up anthropogenic carbon and to transport it to the abyss. The evolution in global open water dissolution is more complex in the versions that include the dependency of production on saturation. Global $CaCO_3$ dissolution is projected to decrease until 2100 in response to decreased $CaCO_3$ export. Then, open water dissolution increases and raises well above the pre-industrial level, mainly in response to decreasing deep ocean saturation. The ratio between open water dissolution to production increases first gradually until the year 2100, then rapidly until the year 2200, followed by a slight trend to reach ~90–95% for all versions. In other words, the fraction of $CaCO_3$ that is dissolved in the open water increases from pre-industrial ~40% for the calcite-only versions and ~60% for the versions including aragonite to almost 100%. Obviously, the expansion of the volume of undersaturated water with respect to aragonite from pre-industrial 40% to around 80% (and with respect to calcite from pre-industrial 20% to 60%) of the total ocean volume causes a corresponding increase in open water $CaCO_3$ dissolution. Trends in production and dissolution are getting smaller towards 2500, but the system is still away from equilibrium by the end of the simulation as expected from the century to multi-millennial perturbation life time of an anthropogenic CO_2 perturbation.

4.2.3 CO_2-$CaCO_3$ production/dissolution feedback on atmospheric CO_2

Anthropogenic emissions cause atmospheric CO_2 to rise, carbon uptake by the ocean to increase, and carbonate ion concentration and the saturation state with respect to

BGD
7, 7029–7090, 2010

$CaCO_3$ to decrease. In response, production and dissolution of $CaCO_3$ change and affect the concentration of DIC and alkalinity, and in turn, the CO_2 partial pressure in surface water and CO_2 uptake by the ocean. Finally, the altered ocean uptake leads to a different evolution of atmospheric CO_2 as compared to a situation where the $CaCO_3$ cycle would not respond to changes in CO_2 and the saturation state. The production of $CaCO_3$ removes DIC, but twice as much alkalinity from the water; the combined effect of removing DIC and alkalinity is to increase pCO_2 (Frankignoulle et al., 1994). Thus, a decrease in $CaCO_3$ production and the related increase in DIC and alkalinity, tends to increase carbon uptake and thus to lower atmospheric CO_2. Similarly, shallower dissolution of $CaCO_3$ tends to increase DIC, alkalinity in surface water and to lower pCO_2 in surface waters and in the atmosphere. In the following, we will quantify the CO_2-$CaCO_3$ production/dissolution feedback with respect to changes in $CaCO_3$ production only by taking the difference between a model version that includes a dependency of $CaCO_3$ production on saturation state and the corresponding version (NODEP) that does not incorporate such a dependency.

The feedback responses in atmospheric CO_2 are −2.5 to −11.4 ppm by 2100 for the High scenario. Thus, the feedback is small compared to the total atmospheric CO_2 perturbation of about 710 ppm by the year 2100 (Table 3, Fig. 9f), despite that $CaCO_3$ production has decreased between 20 and 66% in the different versions. The feedback increases after year 2100, although emissions have been set to zero and $CaCO_3$ production increases again (Fig. 9c). This increase is linked to the slow time scale of surface-to-deep transport in the ocean, and the complex interplay between tracer transport, production, and shallow dissolution of $CaCO_3$. Both model versions with aragonite, CALARAG and CAL2ARAG, provide a feedback on the atmospheric CO_2 of −5.8 ppm by the year 2100. The further evolution is also similar between the two versions. After the peak around year 2200 follows a reduction in feedback towards the year 2500, which is substantially stronger than in the versions with calcite only. This reflects a faster recovery of the carbonate system when aragonite is considered, due to the higher solubility of aragonite compared to calcite. By the year 2500, most model

BGD
7, 7029–7090, 2010

versions provide a feedback effect due to decreasing calcification of between 5.1 and 10.9 ppm. The more extreme parameterization (Lin1) yields a stronger CO_2-$CaCO_3$ production/dissolution feedback corresponding to 24.3 ppm by this time. The feedback effects of the model versions with aragonite, CALARAG and CAL2ARAG, correspond to 6.8 and 6.0 ppm, respectively.

In conclusion, despite the wide range of parameterizations and model versions that are included in our study, the changes in $CaCO_3$ production (and dissolution) resulting from ocean acidification provide only a small overall negative feedback on the atmospheric CO_2.

4.2.4 Sensitivity to future CO_2 emissions

This section addresses the sensitivity of the marine carbonate cycle to projected atmospheric CO_2 trajectories. We focus on the legacy of historical and future CO_2 emissions in terms of impacts on the production/dissolution of marine carbonates (Fig. 13c and d), as well as on the surface ocean saturation state with respect to aragonite (Fig. 13b). To this end we compare the business-as-usual IPCC scenario RCP8.5 (referred to as High) to the alternative pathway RCP6 (Medium) and to a Low scenario. For the High scenario, total cumulative CO_2 emissions of 1916.9 Pg C between 2007 and 2100 translate into a maximum of atmospheric CO_2 of 992 ppm in the year 2100. Atmospheric CO_2 peaks at 702 ppm in 2100 for the Medium scenario (with total cumulative CO_2 emissions of 1138.0 Pg C for the period 2007–2100). In contrast to the High and Medium cases for which emissions increase up to the year 2100 and are then set to zero, the emissions are set to zero after the year 2007 for the Low scenario.

Plotting surface ocean saturation state, $CaCO_3$ production, respectively dissolution as a function of atmospheric CO_2 allows to identify time lags in the system response to the perturbation. The saturation state with respect to aragonite closely follows atmospheric CO_2 (Fig. 13b) suggesting it to be approximately in equilibrium with atmospheric forcing. We observed a small shift towards lower values of the saturation state

BGD
7, 7029–7090, 2010

at identical atmospheric CO_2 values before and after 2100 attributed to the ongoing uptake of CO_2 by the ocean and related changes in carbonate chemistry.

In order to relate changes in surface ocean saturation state with respect to aragonite to habitat suitability for calcifiers, we follow the classification proposed by Kleypas et al. (1999) for tropical coral ecosystems and applied by others at the scale of the global ocean (Steinacher et al., 2009; Frölicher and Joos, 2010). Following this scheme and in terms of carbonate chemistry, $\Omega_A > 4$ stands for optimal, $3 < \Omega_A < 4$, for adequate conditions. While $2 < \Omega_A < 3$ and $1 < \Omega_A < 2$ are indicative of a marginal, respectively inadequate carbonate chemistry for coral growth. Finally values of $\Omega_A < 1$ indicate undersaturated conditions and hence an unsuitable environment for most calcifiers (e.g. pteropods). We stress that uncertainties with ecosystem impacts are large. The high case scenario projects large and, over the duration of the simulation, irreversible changes in surface ocean saturation state. "Suitable habitats" for tropical corals ($3 < \Omega_A > 4$) are lost and conditions remain at "best marginal" ($2 < \Omega_A < 3$) by the year 2500. Our model results further confirm the early onset and persistence of undersaturation of high latitude waters (Orr et al., 2005; Steinacher et al., 2009). The evolution of Ω_A is projected to be less severe in the medium case emission scenario. While carbonate chemistry shifts towards "marginal conditions" for tropical coral growth are around 2100, the saturation state of low latitude waters increases back to values above 3 by the year 2500. Similarly, the extension and duration of undersaturation in high latitude regions is less severe. Keeping in mind the scarcity of data on consequences of large decreases in saturation state for calcifying organisms and from a safety principle, only the low emission scenario allows for moderate changes in Ω_A and hence the prevalence of suitable conditions for marine calcifiers.

As the atmospheric CO_2 increases, the global mean $CaCO_3$ production decreases at the same rate for all three emission scenarios, until the peak CO_2 values of 992 ppm (High), 702 ppm (Medium) and 342 ppm (Low) are reached. Thereafter, the production increases following nearly the same curves back towards, but without reaching, the original $CaCO_3$ production values. This is a direct consequences of the still higher

BGD
7, 7029–7090, 2010

pCO_2 levels in 2500 and hence the lower surface ocean saturations. The dissolution decreases steadily with increasing atmospheric CO_2 due to the reduced supply of $CaCO_3$ particles (Fig. 13c), also increasing again after the peak of atmospheric CO_2 is reached. However, it increases at a larger rate than it decreased and the dissolution rate by the year 2500 becomes much higher than it was initially. While the global mean dissolution rate was around 0.6 Pg C yr^{-1} at the start of the scenarios, it reaches between 0.65 (Low) and 0.75 (Medium and High) Pg C yr^{-1} by the end of the scenario. This non-linearity occurs because, contrary to the $CaCO_3$ production, the $CaCO_3$ dissolution takes place in the deep ocean. Whereas the surface ocean CO_2 concentration is nearly in equilibrium with the atmospheric CO_2, the deep ocean chemistry recovers much more slowly from the CO_2 perturbation.

The resulting feedbacks on atmospheric CO_2 for the 3 scenarios are given in Table 3. Compared to the High scenario which provides a reduction in atmospheric CO_2 of about 5.7 ppm by the year 2100 and 6.8 ppm by the year 2500 due to decreasing calcification and increasing dissolution, the Medium and Low scenarios produce the respective negative feedbacks on atmospheric CO_2 of 4.1 and 1.3 ppm by the year 2100, and 5.0 and 0.8 ppm by the year 2500.

Figure 14 presents the evolution of surface ocean Ω_A (annual mean) with time for the three CO_2 emission scenarios and with the CALARAG model version. Having already described the changes with the High scenario (Fig. 10), the Medium and Low scenarios provide corresponding changes to saturation state. In the Medium scenario (Fig. 14b), the undersaturation starts in Arctic and the Southern Ocean and is only slightly later than with the High scenario. Although a much smaller area of the higher latitudes become undersaturated, the undersaturation in Arctic is maintained for several centuries in both the High and Medium scenario. The Low scenario provides oversaturation everywhere in the surface areas. With this scenario, the surface waters start to recover already soon after the year 2,000 when the saturation state of the surface waters slowly returns towards near-pre-industrial values. However, even with the Low scenario, the pre-industrial values are not reached within the year 2500 in most regions. In line with

BGD
7, 7029–7090, 2010

other studies (e.g. Frölicher and Joos, 2010), the results indicate that future anthropogenic CO_2 emissions may lead to irreversible changes in Ω_A for several centuries.

5 Discussion and conclusions

5.1 Sensitivity of the marine carbonate cycle to parameterizations

Despite the continuously increasing amount of published data about the response of phytoplankton to decreasing saturation state (e.g. Casareto et al., 2009; Godoi et al., 2009; Gao et al., 2009; Shi et al., 2009; Müller et al., 2010), there are still uncertainties related to the future evolution of calcification rates. The magnitude and shape of the dependency of calcification on saturation state are likely to vary with plankton species and group, which makes it difficult to single out a unique parameterization suitable for biogeochemical models. Global biogeochemical models deal with carbonate production as a biogeochemical function rather than attempting to reproduce the complexity of biological responses. Changes in the marine biogeochemical cycle of carbonate in response to ocean acidification and related feedbacks to atmospheric CO_2 have to date been addressed by a limited number of model studies. The comparison between our new results and published data allows us to assess the sensitivity of the marine carbonate cycle to the parameterization of carbonate production and to evaluate the uncertainty associated with that particular process in future projections.

The decrease in calcite production projected by the Bern3D/PISCES model ranges from 20–34% up to 66% for the linear parameterization forced through the intercept. Gehlen et al. (2007) reported a decrease in production equal to 27% by the end of their scenario, where the atmospheric CO_2 was increased at a rate of 1% per year, which is higher than the rate of increase of the IPCC RCP8.5 scenario selected for this study. It resulted in shorter time duration, and the atmospheric concentration reached a maximum of 1144 ppm after 140 years (compared to 992 ppm in our study). Although not directly comparable due to the differences in the underlying scenario and its duration,

BGD
7, 7029–7090, 2010

we note the agreement with our result for the same parameterization. Heinze (2004) projects a decrease in calcification of approximately 30% at atmospheric CO_2 concentrations equal to 1000 ppm, when fitting a linear dependency to the $CaCO_3$ production rates as a function of CO_2 reported by Riebesell et al. (2000). Ridgwell et al. (2007) fitted a first order rate equation to data from a range of studies on coccolithophores and foraminifers. They report a larger reduction in $CaCO_3$ export production of about 60% at an atmospheric CO_2 content equal to 1000 ppm. This value is comparable to our estimate obtained for the linear parameterization forced to the intercept (Lin1). While the parameterization Lin1 provides a poor fit to the data and should be viewed as an extreme end-member for the sensitivity study, such a strong response of calcification on saturation state can a priori not be ruled out based on Ridgwell et al. (2007). Based on available evidence, a global decrease in pelagic carbonate production of about 30% in response to ocean acidification under a business-as-usual-scenario (without climate change) seems likely by the year 2100. However, uncertainties in these estimates are large.

One important question is how species may adapt to the changing environments. Another question is whether the calcifiers use carbonate ions or bicarbonate ions to produce $CaCO_3$ (Bernard et al., 2009). Whereas several studies of coccolithophores, pteropods, foraminifers and corals presented decreasing calcification with decreasing carbonate ion concentrations or saturation state (e.g. Riebesell et al., 2000; Zondervan et al., 2002; Comeau et al., 2009; Spero et al., 1997; Gattuso et al., 1998; Langdon and Atkinson, 2005), a study by Jury et al. (2009) showed that the coral Madracis mirabilis responded strongly to changes in HCO_3^-, but demonstrated very little response if any to changes in CO_3^{2-}, aragonite saturation state or pH. For those species that are more sensitive to changes in HCO_3^- rather than to changes in CO_3^{2-}, the impacts on $CaCO_3$ production, dissolution and corresponding feedbacks will be much smaller, if any at all, due to the practically unlimited amount of HCO_3^- in ocean water.

Next to the shape of the relationship between seawater saturation state and pelagic carbonate production, the functional group to which it is assigned, as well as the

BGD
7, 7029–7090, 2010

particular $CaCO_3$ polymorph produced are at the origin of uncertainties in model projections. Concerning calcifying zooplankton, such as pteropods and foraminifers, even fewer experimental data are available. Since the sensitivity study discussed above demonstrated an overall low sensitivity of the carbonate cycle to the shape of the parameterization, we adopted a linear curve to describe the response of calcifying mesozooplankton to decreasing saturation state. By including the more soluble aragonite, as well as calcite producing mesozooplankton, we increase the sensitivity of $CaCO_3$ production to increasing atmospheric CO_2. The Bern3D/PISCES model version CALARAG (calcite produced by nanophytoplankton and aragonite by mesozooplankton) projects a larger reduction in total $CaCO_3$ production (−35%) by the year 2100 than obtained with the NEMO/PISCES model (−19%) for a similar parameterization (Gangstø et al., 2008). The stronger response of the Bern3D model might be related to differences in (i) the modeled pre-industrial saturation horizon, (ii) the rate of transfer of anthropogenic CO_2 from the surface to the deep ocean (ventilation, deep convection) and finally to differences in the emission scenarios. Scenario RCP8.5 yields atmospheric CO_2 levels about 165 ppm higher by the year 2100 than SRESA2 (Gangstø et al., 2008). The large differences obtained with the same biogeochemical model, but coupled to different ocean general circulation models highlights the need for a systematic model inter-comparison study.

5.2 Sensitivity of the marine carbonate cycle to emission scenarios

We quantified changes in the marine $CaCO_3$ cycle for two emission commitment scenarios in which carbon emissions followed RCP8.5 (High) and RCP6 (Medium) until 2100 and are set to zero after 2100, and one scenario where the emissions are set to zero after the year 2007 (Low). In all simulations, the surface aragonite saturation state decreases in parallel to increasing atmospheric CO_2. The resulting decreases in $CaCO_3$ production and increases in dissolution have a negligible effect on surface ocean carbonate chemistry. Ongoing ocean acidification is thus not buffered by changes in $CaCO_3$ production and dissolution. Under the High scenario,

BGD
7, 7029–7090, 2010

undersaturation of Arctic and Southern Ocean surface waters is projected within few decades, and is maintained over several centuries. In the Arctic, both the Medium and the High scenario give early and long-term undersaturation. Although undersaturation of the surface waters is overall not reached under the Low scenario, we note that the saturation state remains below pre-industrial levels by the year 2500. The results confirm previous studies (Orr et al., 2005; Steinacher et al., 2009; Froelicher et al., 2010) indicating that future anthropogenic CO_2 emissions may lead to irreversible changes in Ω_A for several centuries.

The projected changes in saturation state and decreasing calcification may have large consequences for marine organisms (Fabry et al., 2008; Guinotte and Fabry, 2008; Raven et al., 2005; Kleypas et al., 2006). When interpreting our results in the light of a classification of surface ocean saturation state with respect to aragonite in terms of suitability to marine calcifiers, both scenarios High and Medium suggest large scale habitat loss to occur within a few decades and prevailing up to several centuries. Following the precautionary principle, only scenarios with low carbon emissions seem recommendable when large scale changes in ocean ecosystems and their functioning are to be avoided.

The legacy of ocean acidification and ongoing CO_2 uptake after the unrealistic shutdown of emissions after 2100 is also seen in the deep ocean. The volume of undersaturated water masses remain superior to its pre-industrial value by the year 2500. As a consequence of the slow recovery of the deep ocean after a CO_2 perturbation, the $CaCO_3$ dissolution of all model versions continues to increase over the scenario. By the end of the High scenario, the $CaCO_3$ dissolution-production ratio has stabilized at a value that is 30–50% higher than its initial value. Changes in $CaCO_3$ production will lead to rain ratio changes, which together with a reduction in $CaCO_3$ sedimentation and burial will modify the marine carbonate cycle for several thousands year. The interaction with marine sediments will ultimately bring the system back to a new equilibrium state (Archer, 2005).

BGD
7, 7029–7090, 2010

5.3 Feedback quantification

When it comes to the CO_2-$CaCO_3$ production/dissolution feedback, our results fall in a narrow range considering the variety of model parameterizations and emission scenarios addressed in this study. They range from −6 to −26 Pg C by the year 2500, in the case of continuous CO_2 emissions up to the year 2100. Our results compare well to previous studies which report negative feedbacks to atmospheric CO_2 extending from −5 to −26 Pg C integrated over the duration of the simulations (Heinze, 2004; Gehlen et al., 2007; Ridgwell et al., 2007; Hofmann and Schellnhuber, 2009). Despite the diversity in model systems, scenarios and parameterizations all studies converge to project a rather modest negative CO_2-$CaCO_3$ production/dissolution feedback to increasing atmospheric CO_2.

Climate change impacts with increasing atmospheric CO_2, are not included in this model setup. PISCES includes only an indirect approach to the ballast effect, and may thus not fully account for the expected decrease in ballasting of organic C fluxes by $CaCO_3$ (Armstrong et al., 2002; Klaas and Archer, 2002) as a direct consequence of ocean acidification. A reduction in the ballast effect would decrease the penetration depth of organic C. The resulting shallower remineralization depth of organic C would provide a positive feedback to atmospheric CO_2, which might well be of similar or larger magnitude as the CO_2-$CaCO_3$ production/dissolution feedback (Barker et al., 2002; Heinze et al., 2004; Hofmann and Schnellnhuber, 2009; Kwon et al., 2009).

Climate change, with higher temperatures is at the origin of an increase in stratification of the ocean waters. Chemical changes related to the temperature effect (decreasing solubility of CO_2 with increasing water temperature), but also a slowing down of the surface to deep transport of water masses, combine to a positive feedback to the atmospheric CO_2 (Joos et al., 1999; Greenblatt and Sarmiento, 2004; Friedlingstein et al., 2006; Plattner et al., 2008.).

Impacts of climate change on saturation are small except in polar waters. The decrease in Ω_A in the Arctic is amplified by surface freshening and sea ice retreat which

BGD
7, 7029–7090, 2010

causes increased uptake of anthropogenic carbon (Steinacher et al., 2009). Going along with the projected increase in stratification may be a reduction in marine net primary productivity and export production (Steinacher et al., 2010). The reorganization of surface ocean ecosystems with a shift from diatoms towards nanophytoplankton (Bopp et al., 2006) has also been suggested. The ultimate fate of $CaCO_3$ production will thus depend on the interplay between ocean acidification and direct climate change effects. While this discussion highlights the large uncertainties still linked to projections of changes in the marine carbonate cycle and associated feedbacks to atmospheric CO_2, it also suggests that the magnitude of published feedback estimates might represent an upper limit on time scales of decades to a few centuries.

Acknowledgements. The study was supported by the EU projects EUROCANS (511106-2), CARBOOCEAN (511176-2) and EPOCA (FP7/2007-2013; no. 211384), and the Swiss National Science Foundation. We would like to thank Olivier Aumont for providing the PISCES model, and Marco Steinacher and Kay Bieri for technical assistance. Thanks to J. Büdenbender, S. Lischka and U. Riebesell for access to unpublished data from their study on pteropods in Kongsfjorden.

The publication of this article is financed by CNRS-INSU.

BGD
7, 7029–7090, 2010

References

Accornero, A., Manno, C., Esposito, F., and Gambi, M. C.: The vertical flux of particulate matter in the polynya of Terra Nova Bay, Part II, Biological components, Antarct. Sci., 15(2), 175–188, 2003.

Archer, D.: Fate of fossil fuel CO_2 in geologic time, J. Geophys. Res., 110, C09S05, doi:10.1029/2004JC002625, 2005.

Armstrong, R. A., Lee, C., Hedges, J. I., Honjo, S., and Wakeham, S. G.: A new, mechanistic model for organic carbon fluxes in the ocean based on the quantitative association of POC with ballast minerals, Deep-Sea Res. Pt. II, 49, 219–236, 2001.

Aumont, O., Maier-Reimer, E., Blain, S., and Monfray, P.: An ecosystem model of the global ocean including Fe, Si, P colimitations, Global Biogeochem. Cy., 17(2), GB1060, doi:10.1029/2001GB001745, 2003.

Aumont, O. and Bopp, L.: Globalizing results from ocean in situ iron fertilization studies, Global Biogeochem. Cy., 20, GB2017, doi:10.1029/2005GB002591, 2006.

Balch, W., Drapeau, D., Bowler, B., and Booth, E.: Prediction of pelagic calcification rates using satellite measurements, Deep-Sea Res. Pt. II, 54(5–7), 478–495, 2007.

Barker, S., Higgins, J. A., and Elderfield, H.: The future of the carbon cycle: review, calcification response, ballast and feedback on atmospheric CO_2, Philosophical Transactions: Mathematical, Physical and Engineering Sciences, 361, 1977–1999.

Berelson, W. M., Balch, W. M., Najjar, R., Feely, R. A., Sabine, C., and Lee, K.: Relating estimates of $CaCO_3$ production, export, and dissolution in the water column to measurements of $CaCO_3$ rain into sediment traps and dissolution on the sea floor: A revised global carbonate budget, Global Biogeochem. Cy., 21, GB1024, doi:10.1029/2006GB002803, 2007.

Berger, W. H.: Deep-Sea carbonate: Pteropod distribution and the aragonite compensation depth, Deep-Sea Res., 25, 447–452, 1978.

Berner, R. A.: Sedimentation and Dissolution of Pteropods in the Ocean, in: The Fate of Fossil Fuel CO_2 in the Oceans, edited by: Andersen, N. R. and Malahoff, A., Plenum Press, New York, 243–260, 1977.

Berner, R. A. and Honjo, S.: Pelagic sedimentation of aragonite: its geochemical significance, Science, 211, 940–942, 1981.

BGD
7, 7029–7090, 2010

Bijma, J., Spero, H. J., and Lea, D. W.: Reassessing foraminiferal stable isotope geochemistry: Impact of the oceanic carbonate system (experimental results), in :Use of Proxies in Paleoceanography: Examples From the South Atlantic, edited by: Fischer, G. and Wefer, G., Springer, New York, 489–512, 1999.

Bopp, L., Aumont, O., Cadule, P., Alvain, S., and Gehlen, M.: Response of diatoms distribution to global warming and potential implications: A global model study, Geophys. Res. Lett., 32(19), L19606, doi:10.1029/2005GL019606, 2005.

Bryan, F.: High-latitude salinity effects and interhemispheric thermohaline circulations, Nature, 323, 301–304, 1986.

Buitenhuis, E., Le Quéré, C., Aumont, O., Beaugrand, G., Bunker, A., Hirst, A., Ikeda, T., O'Brien, T., Piontkovski, S., and Straile, D.: Biogeochemical fluxes through mesozooplankton, Global Biogeochem. Cy., 20, GB2003, doi:10.1029/2005GB002511, 2006.

Casareto, B. E., Niraula, M. O., Fujimura, H., and Suzuki, Y.: Effects of carbon dioxide on the coccolithophorid *Pleurochrysis carterae* in incubation experiments, Aquat. Biol., 7, 59–70, 2009.

Collier, R., Dymond, J., Honjo, S., Manganini, S., Francois, R., and Dunbar, R.: The vertical flux of biogenic and lithogenic material in the Ross Sea: moored sediment trap observations 1996–1998, Deep-Sea Res. Py. II, 47, 3491–3520, 2000.

Comeau, S., Gorsky, G., Jeffree, R., Teyssié, J.-L., and Gattuso, J.-P.: Impact of ocean acidification on a key Arctic pelagic mollusc (*Limacina helicina*), Biogeosciences, 6, 1877–1882, doi:10.5194/bg-6-1877-2009, 2009.

Delille, B., Harlay, J., Zondervan, I., Jacquet, S., Chou, L., Wollast, R., Bellerby, R. G. J., Frankignoulle, M., Borges, A. V., Riebesell, U., and Gattuso, J.-P.: Response of primary production and calcification to changes of pCO_2 during experimental blooms of the coccolithophorid *Emiliania huxleyi*, Global Biogeochem. Cy., 19, GB2023, doi:10.1029/2004GB002318, 2005.

Dissard, D., Nehrke, G., Reichart, G. J., and Bijma, J.: Impact of seawater pCO_2 on calcification and Mg/Ca and Sr/Ca ratios in benthic foraminifera calcite: results from culturing experiments with *Ammonia tepida*, Biogeosciences, 7, 81–93, doi:10.5194/bg-7-81-2010, 2010.

Edwards, N. R., Wilmott, A. J., and Killworth, P. D.: On the role of topography and wind stress on the stability of the thermohaline circulation, J. Phys. Oceanogr., 28, 756–778, 1998.

BGD

7, 7029–7090, 2010

Edwards, N. R. and Marsh, R.: Uncertainties due to transport-parameter sensitivity in an efficient 3-D ocean-climate model, Clim. Dynam., 24(4), 415–433, doi:10.1007/s00382–004–0508–8, 2005.

Fabry, V. J.: Shell growth rates of pteropod and heteropod mollusks and aragonite production in the open ocean: Implications for the marine carbonate system, J. Mar. Res., 48, 209–222, 1990.

Fabry, V. J. and Deuser, W. G.: Aragonite and magnesium calcite fluxes to the deep Sargasso Sea, Deep-Sea Res Pt. I, 38(6), 713–728, 1991.

Fabry, V. J., Seibel, B. A., Feely, R. A., and Orr, J. C.: Impacts of ocean acidification on marine fauna and ecosystem processes, ICES J. Mar. Sci., 65, 414–432, 2008.

Feely, R. A., Sabine, C. L., Lee, K., Berelson, W., Kleypas, J., Fabry, V. J., and Millero, F. J.: Impact of anthropogenic CO_2 on the $CaCO_3$ system in the oceans, Science, 305, 362–366, 2004.

Frankignoulle, M. and Canon, C.: Marine calcification as a source of carbon dioxide: Positive feedback of increasing atmospheric CO_2, Limnol. Oceanogr., 39(2), 458–462, 1994.

Friedlingstein, P., Cox, P., Betts, R., Bopp, L., von Bloh, W., Brovkin, V., Cadule, P., Doney, S., Eby, M., Fung, I., Bala, G., John, J., Jones, C., Joos, F., Kato, T., Kawamiya, M., Knorr, W., Lindsay, K., Matthews, H. D., Raddatz, T., Rayner, P., Reick, C., Roeckner, E., Schnitzler, K.-G., Schnur, R., Strassmann, K., Weaver, A. J., Yoshikawa, C., and Zeng, N.: Climate-carbon cycle feedback analysis: Results from the C4MIP model intercomparison, J. Climate, 19(14), 3337–3353, 2006.

Frölicher, T. L. and Joos, F.: Reversible and irreversible impacts of greenhouse gas emissions in multi-century projections with a comprehensive climate-carbon model, Clim. Dynam., in press, doi:10.1007/s00382-009-0727-0, 2010.

Gangstø, R., Gehlen, M., Schneider, B., Bopp, L., Aumont, O., and Joos, F.: Modeling the marine aragonite cycle: changes under rising carbon dioxide and its role in shallow water $CaCO_3$ dissolution, Biogeosciences, 5, 1057–1072, doi:10.5194/bg-5-1057-2008, 2008.

Gao, K. S., Ruan, Z. X., Villafane, V. E., Gattuso, J.-P., and Helbling, E. W.: Ocean acidification exacerbates the effect of UV radiation on the calcifying phytoplankter *Emiliania huxleyi*, Limnol. Oceanogr., 54(6), 1855–1862, 2009.

Gattuso, J.-P., Frankignoulle, M., Bourge, I., Romaine, S., and Buddemeier, R. W.: Effect of calcium carbonate saturation of seawater on coral calcification, Global Planet. Change, 18, 37–46, 1998.

BGD

7, 7029–7090, 2010

Gehlen, M., Bopp, L., Emprin, N., Aumont, O., Heinze, C., and Ragueneau, O.: Reconciling surface ocean productivity, export fluxes and sediment composition in a global biogeochemical ocean model, Biogeosciences, 3, 521–537, doi:10.5194/bg-3-521-2006, 2006.

Gehlen, M., Gangstø, R., Schneider, B., Bopp, L., Aumont, O., and Ethe, C.: The fate of pelagic $CaCO_3$ production in a high CO_2 ocean: a model study, Biogeosciences, 4, 505–519, doi:10.5194/bg-4-505-2007, 2007.

Gerber, M., Joos, F., Vazquez Rodriguez, M., Touratier, F., and Goyet, C.: Regional air-sea fluxes of anthropogenic carbon inferred with an Ensemble Kalman Filter, Global Biogeochem. Cy., 23, GB1013, doi:10.1029/2008GB003247, 2009.

Gerber, M. and Joos, F.: Carbon sources and sinks from an Ensemble Kalman Filter ocean data assimilation, Global Biogeochem. Cy., 24, GB3004, doi:10.1029/2009GB003531, 2010.

Griffies, S. M.: The Gent-McWilliams skew flux, J. Phys. Oceanogr., 28, 831–841, 1998.

Godoi, R. H. M., Aerts, K., Harlay, J., Kaegi, R., Ro, C.-U., Chou, L., and Van Grieken, R.: Organic surface coating on Coccolithophores - *Emiliania huxleyi*: Its determination and implication in the marine carbon cycle, Microchem. J., 91(2), 266–271, 2009.

Goyet, C., Healy, R. J., and Ryan, J. P.: Global distribution of total inorganic carbon and total alkalinity below the deepest winter mixed layer depths, ORNL/CDIAC-127, NDP-076, Carbon Dioxide Information Analysis Center, Oak Ridge National Laboratory, US Department of Energy, Oak Ridge, Tennessee, 2000.

Greenblatt, J. and Sarmiento, J.: Variability and climate feedback mechanisms in ocean uptake of CO_2, in: The Global Carbon Cycle: Integrating Humans, Climate, and the Natural World, edited by: Field, C. B. and Raupach, M. R., Scope 62, Island Press, Washington, DC, 257–275, 2004.

Heinze, C.: Simulating oceanic $CaCO_3$ export production in the greenhouse, Geophys. Res. Let., 31, L16308, doi:10.1029/2004GL020613, 2004.

Hofmann, M. and Schellnhuber, H.-J.: Oceanic acidification affects marine carbon pump and triggers extended marine oxygen holes, P. Natl. Acad. Sci., 106, 3017–3022, 2009.

Honjo, S., Francois, R., Manganini, S., Dymond, J., and Collier, R.: Particle fluxes to the interior of the Southern Ocean in the Western Pacific sector along 170° W, Deep-Sea Res. Pt. II, 47, 3521–3548, 2000.

Honjo, S.: Particle export and the biological pump in the Southern Ocean, Antarct. Sci., 16(4), 501–516, 2004.

BGD

7, 7029–7090, 2010

Hunt, B. P. V., Pakhomov, E. A., Hosie, G. W., Siegel, V., Ward, P., and Bernard, K.: Pteropods in Southern Ocean ecosystems, Prog. Oceanogr., 78(3), 193–221, 2008.

Iglesias-Rodriguez, M. D., Armstrong, R., Feely, R., Hood, R., Kleypas, J., Milliman, J. D., Sabine, C., and Sarmiento, J.: Representing key phytoplankton functional groups in oceanic carbon cycle models: Coccolithophorids, Global Biogeochem. Cy., 16, 1100, doi:10.1029/2001GB001454, 2002a.

Iglesias-Rodriguez, M. D., Armstrong, R., Feely, R., Hood, R., Kleypas, J., Milliman, J. D., Sabine, C., and Sarmiento, J.: Progress made in study of ocean's calcium carbonate budget, EOS, 83(34), 374–375, 2002b.

Iglesias-Rodriguez, M. D., Halloran, P. R., Rickaby, R. E. M., Hall, I. R., Colmenero-Hidalgo, E., Gittins, J. R., Green, D. R. H., Tyrrell, T., Gibbs, S. J., von Dassow, P., Rehm, E., Armbrust, E. V., and Boessenkool, K. P.:, Phytoplankton calcification in a high-CO_2 world, Science, 320, 336–340, 2008.

Jin, X., Gruber, N., Dunne, J. P., Sarmiento, J. L., and Armstrong, R. A.: Diagnosing the contribution of phytoplankton functional groups to the production and export of particulate organic carbon, $CaCO_3$, and opal from global nutrient and alkalinity distributions, Global Biogeochem. Cy., 20, GB2015, doi:10.1029/2005GB002532, 2006.

Joos, F., Plattner, G.-K., Stocker, T. F., Marchal, O., and Schmittner, A.: Global warming and marine carbon cycle feedbacks on future atmospheric CO_2, Science, 284/5413, 464–467, 1999.

Jury, C. P., Whitehead, R. F., and Szmant, A. M.: Effects of variations in carbonate chemistry on the calcification rates of Madracis auretenra (= Madracis mirabilis sensu Wells, 1973): bicarbonate concentrations best predict calcification rates, Global Change Biol., 16(5), 1632–1644, doi:10.1111/j.1365-2486.2009.02057.x, 2010.

Key, R. M., Kozyr, A., Sabine, C. L., Lee, K., Wanninkhof, R., Bullister, J. L., Feely, R. A., Millero, F. J., Mordy, C., and Peng, T.-H.: A global ocean carbon climatology: Results from Global Data Analysis Project (GLODAP), Global Biogeochem. Cy., 18, GB4031, doi:10.1029/2004GB002247, 2004.

Klaas, C. and Archer, D.: Association of sinking organic matter with various types of mineral ballast in the deep sea: Implications for the rain ratio, Global Biogeochem. Cy., 16(4), 1116, doi:10.1029/2001GB001765, 2002.

BGD

7, 7029–7090, 2010

Kleypas, J. A., Buddemeier, R. W., Archer, D., Gattuso, J.-P., Langdon, C., and Opdyke, B. N.: Geochemical consequences of increased atmospheric carbon dioxide on coral reefs, Science, 284, 118–120, 1999.

Kleypas, J. A., Feely, R. A., Fabry, V. J., Langdon, C., Sabine, C. L., and Robbins, L. L.: Impacts of ocean acidification on coral reefs and other marine calcifiers: A guide for future research, report of a workshop held 18–20 April 2005, St. Petersburg, FL, sponsored by NSF, NOAA, and the US Geological Survey, 88 pp., 2006.

Kuroyanagi, A., Kawahata, H., Suzuki, A., Fujita, K., and Irie, T.: Impacts of ocean acidification on large benthic foraminifers: Results from laboratory experiments, Mar. Micropaleontol., 73(3–4), 190–195, doi:10.1016/j.marmicro.2009.09.003, 2009.

Kwon, E. Y., Primeau, F., and Sarmiento, J. L.: The impact of remineralization depth on the air-sea carbon balance, Nat. Geosci., 2, 630–635 doi:10.1038/ngeo612, 2009.

Lalli, C. M. and Gilmer, R. W.: Pelagic snails: The Biology of Holoplanktonic Gastropod Mollusks, Stanford University Press, 1989.

Langer, G., Geisen, M., Baumann, K.-H., Kläs, J., Riebesell, U., Thoms, S., and Young, J. R.: Species-specific responses of calcifying algae to changing seawater carbonate chemistry, Geochem. Geophy. Geosy., 7, Q09006, doi:10.1029/2005GC001227, 2006.

Langdon, C., Broecker, W. S., Hammond, D. E., Glenn, E., Fitzsimmons, K., Nelson, S. G., Peng, T.-H., Hajdas, I., and Bonani, G.: Effect of elevated CO_2 on the community metabolism of an experimental coral reef, Global Biogeochem. Cy., 17(1), 1011, doi:10.1029/2002GB001941, 2003.

Langdon, C. and Atkinson, M. J.: Effect of elevated pCO_2 on photosynthesis and calcification of corals and interactions with seasonal change in temperate/irradiance and nutrient enrichment, J. Geophys. Res., 110, C09S07, doi:10.1029/2004JC002576, 2005.

Lee, K.: Global net community production estimated from the annual cycle of surface water total dissolved inorganic carbon, Limnol. Oceanogr., 46(6), 1287–1297, 2001.

Legendre, L. and Le Févre, J.: Microbial food webs and the export of biogenic carbon in oceans, Aquat. Microb. Ecol., 9, 69–77, 1995.

Lombard, F., da Rocha, R. E., Bijma, J., and Gattuso, J.-P.: Effect of carbonate ion concentration and irradiance on calcification in planktonic foraminifera, Biogeosciences, 7, 247–255, doi:10.5194/bg-7-247-2010, 2010.

Milliman, J. D. and Droxler, A. W.: Neritic and pelagic carbonate sedimentation in the marine environment: ignorance is not bliss, Geol. Rundsch., 85, 496–504, 1996.

BGD

7, 7029–7090, 2010

Moy, A. D., Bray, S. G., Trull, T. W., and Howard, W. R.: Reduced calcification in modern Southern Ocean planktonic foraminifera, Nat. Geosci., 2, 276–280, doi:10.1038/ngeo460, 2009.

Munhoven, G.: Glacial-interglacial rain ratio changes: Implications for atmospheric CO_2 and ocean-sediment interaction, Deep-Sea Res. Pt. II, 54(5–7), 722–746, 2007.

Müller, S. A., Joos, F., Edwards, N. R., and Stocker, T. F.: Water mass distribution and ventilation time scales in a cost-efficient, three-dimensional ocean model, J. Climate, 19(21), 5479–5499, 2006.

Müller, S. A., Joos, F., Plattner, G.-K., Edwards, N. R., and Stocker, T. F.: Modeled natural and excess radiocarbon: sensitivities to the gas exchange formulation and ocean transport strength, Global Biogeochem. Cy., 22, GB3011, doi:10.1029/2007GB003065, 2008.

Müller, M. N., Schulz, K. G., and Riebesell, U.: Effects of long-term high CO_2 exposure on two species of coccolithophores, Biogeosciences, 7, 1109–1116, doi:10.5194/bg-7-1109-2010, 2010.

Najjar, R. G. and Orr, J.: Biotic-HOWTO, technical report, Lab. des Sci. du Clim. et l'Environ., Comm. à l'Energie At. Saclay, available at http://www.ipsl.jussieu.fr/OCMIP/phase2/simulations/Biotic/HOWTO-Biotic.html, last access: September 2010, Gif-sur-Yvette, France, 15 pp., 1999.

Orr, J., Najjar, R. G., Sabine, C. L., and Joos, F.: Abiotic-HOWTO, technical report, Lab. des Sci. du Clim. et l'Environ., Comm. à l'Energie At. Saclay, available at http://www.ipsl.jussieu.fr/OCMIP/phase2/simulations/Abiotic/HOWTO-Abiotic.html, last access: September 2010, Gif-sur-Yvette, France, 25 pp., 1999.

Orr, J. C., Fabry, V. J., Aumont, O., Bopp, L., Doney, S. C., Feely, R. A., Gnanadesikan, A., Gruber, N., Ishida, A., Joos, F., Key, R. M., Lindsay, K., Maier-Reimer, E., Matear, R., Monfray, P., Mouchet, A., Najjar, R. G., Plattner, G.-K., Rodgers, K. B., Sabine, C. L., Sarmiento, J. L., Schlitzer, R., Slater, R. D., Totterdell, I. J., Weirig, M.-F., Yamanaka, Y., and Yool, A.: Antropogenic ocean acidification over the twenty-first century and its impact on calcifying organisms, Nature, 437, 681–686, 2005.

Panchang, R., Nigam, R., Riedel, F., Janssen, A. W., and Ko Yui Hla, U.: A review of the studies on pteropods from the northern Indian Ocean region with a report on the pteropods of Irrawaddy continental shelf off Myanmar (Burma), Indian J. Mar. Sci., 36(4), 384–398, 2007.

BGD

7, 7029–7090, 2010

Parekh, P., Joos, F., and Müller, S. A.: A modeling assessment of the interplay between aeolian iron fluxes and iron-binding ligands in controlling carbon dioxide fluctuations during Antarctic warm events, Paleoceanography, 23, PA4202, doi:10.1029/2007PA001531, 2008.

Plattner, G.-K., Knutti, R., Joos, F., Stocker, T. F., von Bloh, W., Brovkin, V., Cameron, D., Driesschaert, E., Dutkiewiz, S., Eby, M., Edwards, N. R., Fichefet, T., Hargreaves, J. C., Jones, C. D., Loutre, M. F., Matthews, H. D., Mouchet, A., Müller, S. A., Nawrath, S., Price, A., Sokolov, A., Strassmann, K. M., and Weaver, A. J.: Long-term climate commitments projected with climate-carbon cycle models, J. Climate, 21/12, 2721–2751, 2008.

Raven, J. A. and Falkowski, P. G.: Oceanic sinks for atmospheric CO_2, Plant Cell Environ., 22, 741–755, doi:10.1046/j.1365-3040.1999.00419, 1999.

Ridgwell, A., Zondervan, I., Hargreaves, J. C., Bijma, J., and Lenton, T. M.: Assessing the potential long-term increase of oceanic fossil fuel CO_2 uptake due to CO_2-calcification feedback, Biogeosciences, 4, 481–492, doi:10.5194/bg-4-481-2007, 2007.

Ridgwell, A., Schmidt, D. N., Turley, C., Brownlee, C., Maldonado, M. T., Tortell, P., and Young, J. R.: From laboratory manipulations to Earth system models: scaling calcification impacts of ocean acidification, Biogeosciences, 6, 2611–2623, doi:10.5194/bg-6-2611-2009, 2009.

Riebesell, U., Zondervan, I., Rost, B., Tortell, P. D., Zeebe, R. E., and Morel, F. M. M.: Reduced calcification of marine plankton in response to increased atmospheric CO_2, Nature, 407, 364–367, 2000.

Ritz, S. P., Stocker, T. F., and Müller, S. A.: Modeling the effect of abrupt ocean circulation change on marine reservoir age, Earth Planet. Sc. Lett., 268(1–2), 202–211, doi:10.1016/j.epsl.2008.01.024, 2008.

Rowe, G. T., Wei, C., Nunnally, C., Haedrich, R., Montagna, P., Baguley, J. G., Bernhard, J. M., Wicksten, M., Ammons, A., Escobar Briones, E. G., Soliman, Y., and Deming, J.: Comparative biomass structure and estimated carbon flow in food webs in the deep Gulf of Mexico, Deep-Sea Res. Pt. II, 55, 2699–2711, 2008.

Sarmiento, J. L., Dunne, J., Gnanadesikan, A., Key, R. M., Matsumoto, K., and Slater, R.: A new estimate of the $CaCO_3$ to organic carbon export ratio, Global Biogeochem. Cy., 16(4), 1107, doi:10.1029/2002GB001919, 2002.

Schiebel, R.: Planktic foraminiferal sedimentation and the marine calcite budget, Global Biogeochem. Cy., 16(4), 1065, doi:10.1029/2001GB001459, 2002.

BGD
7, 7029–7090, 2010

Sciandra, A., Harlay, J., Lefèvre, D., Lemée, R., Rimmelin, P., Denis, M., and Gattuso, J.-P.: Response of coccolithophorid *Emiliania huxleyi* to elevated partial pressure of CO_2 under nitrogen limitation, Mar. Ecol.-Prog. Ser., 261, 111–222, 2003.

Shi, D., Xu, Y., and Morel, F. M. M.: Effects of the pH/pCO_2 control method on medium chemistry and phytoplankton growth, Biogeosciences, 6, 1199–1207, doi:10.5194/bg-6-1199-2009, 2009.

Siddall, M., Stocker, T. F., Henderson, G. M., Joos, F., Frank, M., Edwards, N. R., Ritz, S. P., and Müller, S. A.: Modeling the relationship between $^{231}Pa/^{230}Th$ distribution in North Atlantic sediment and Atlantic meridional overturning circulation, Paleoceanography, 22, PA2214, doi:10.1029/2006PA001358, 2007.

Spero, H. J., Bijma, J., Lea, D. W., and Bemis, B. E.: Effect of seawater carbonate concentration on foraminiferal carbon and oxygen isotopes, Nature, 390, 497–500, 1997.

Steinacher, M., Joos, F., Frölicher, T. L., Plattner, G.-K., and Doney, S. C.: Imminent ocean acidification in the Arctic projected with the NCAR global coupled carbon cycle-climate model, Biogeosciences, 6, 515–533, doi:10.5194/bg-6-515-2009, 2009.

Steinacher, M., Joos, F., Frölicher, T. L., Bopp, L., Cadule, P., Cocco, V., Doney, S. C., Gehlen, M., Lindsay, K., Moore, J. K., Schneider, B., and Segschneider, J.: Projected 21st century decrease in marine productivity: a multi-model analysis, Biogeosciences, 7, 979–1005, doi:10.5194/bg-7-979-2010, 2010.

Strassmann, K. M., Plattner, G.-K., and Joos, F.: CO_2 and non-CO_2 radiative forcings in climate projections for twenty-first century mitigation scenarios, Clim. Dynam., 33/6, 737–749, 2009.

Talley, L. D., Reid, J. L., and Robbins, P. E.: Data-based meridional overturning streamfunctions for the global ocean, J. Climate, 16, 3213–3226, 2003.

Tschumi, T., Joos, F., and Parekh, P.: How important are Southern Hemisphere wind changes for low glacial carbon dioxide? A model study, Paleoceanography, 23, PA4208, doi:10.1029/2008PA001592, 2008.

Urban-Rich, J., Dagg, M., and Peterson, J.: Copepod grazing on phytoplankton in the Pacific sector of the Antarctic Polar Front, Deep-Sea Res. Pt. II, 48, 4223–4246, 2001.

Volbers, A. N. A.: Planktic foraminifera as paleoceangraphic indicators: Production, preservation, and reconstruction of upwelling intensity, implications from late quarternary South Atlantic sediments, Berichte, Fachbereich Geowissenschaften, Universität Bremen, 184, 114 pp., 2001.

BGD

7, 7029–7090, 2010

Van Vuuren, D. P., Meinshausen, M., Plattner, G.-K., Joos, F., Strassmann, K. M., Smith, S. J., Wigley, T. M. L., Raper, S. C. B., Riahi, K., de la Chesnaye, F., den Elzen, M., Fujino, J., Jiang, K., Nakicenovic, N., Paltsev, S., and Reilly, J. M.: Temperature increase of 21st century mitigation scenarios, P. Natl. Acad. Sci., 105/40, 15258–15262, 2008.

Wolf-Gladrow, D. A., Riebesell, U., Burkhardt, S., and Bijma, J.: Direct effects of CO_2 concentration on growth and isotopic composition of marine plankton, Tellus B, 51(2), 461–476, 1999.

Zondervan, I., Zeebe, R. E, Rost, B., and Riebesell, U.: Decreasing marine biogenic calcification: A negative feedback on rising atmospheric pCO_2, Global Biogeochem. Cy., 15(2) 507–516, 2001.

Zondervan, I., Rost, B., and Riebesell, U.: Effect of CO_2 concentration on the PIC/POC ratio in the coccolithophore *Emiliania huxleyi* grown under light-limiting conditions and different daylengths, J. Exp. Mar. Biol. Ecol., 272, 55–70, 2002.

Zondervan, I.: The effects of light, macronutrients, trace metals and CO_2 on the production of calcium carbonate and organic carbon in coccolithophores – A review, Deep-Sea Res. Pt. II, 54, 521–537, 2007.

BGD

7, 7029–7090, 2010

Table 1. Simulated pre-industrial $CaCO_3$ production (after 3 000 years of integration) for different parameterizations of $CaCO_3$ production in the Bern3D/PISCES model.

Model version	Calcite production ($Pg\,C\,yr^{-1}$)	Aragonite production ($Pg\,C\,yr^{-1}$)	Parameterization of the dependency of $CaCO_3$ production on saturation state
Calcite production by nanophytoplankton only			
CALMIC1	1.0	–	Michaelis-Menten, this study
CALMIC2	1.00	–	Michaelis-Menten based on Gehlen et al. 2007
CALLIN1	1.05	–	Linear curve, forced to zero for $\Omega = 1$
CALLIN2	1.04	–	Linear curve, freely fitted
NODEPC	1.02	–	Production is independent of saturation state
Calcite production by nanophytoplankton and aragonite production by mesozooplankton			
CALARAG	0.66	0.34	Michaelis-Menten (this study) for calcite, linear for aragonite
NODEPCA	0.69	0.35	Production is independent of saturation state
Calcite production by nanophyto- and mesozooplankton and aragonite production by mesozooplankton			
CAL2ARAG	0.33 + 0.31	0.34	Michaelis-Menten for calcite by nanoplankton, linear for aragonite production, linear for calcite production by mesoplankton
NODEPC2A	0.36 + 0.35	0.35	Production is independent of saturation state

BGD
7, 7029–7090, 2010

Table 2. The pre-industrial $CaCO_3$ budget: Results are for different parameterizations of the $CaCO_3$ production in the Bern3D/PISCES model and the NEMO/PISCES model, labeled PISCCAL (Gehlen et al., 2007), and PISC-ARAG (Gangstø et al., 2008). Parameterizations for the carbonate cycle are comparable between versions CAL-MIC and PISC-CAL and between versions CAL-ARAG and PISC-ARAG. The lower boundary represents the deepest model grid boxes. The flux at the lower boundary is not to be compared with estimates of the burial flux; the latter is not modeled in this study. Units are Pg C yr^{-1}.

Parameterization	Bern3D CAL-MIC1	Bern3D CAL-MIC2	Bern3D CAL-ARAG	Bern3D CAL2-ARAG	NEMO PISC-CAL	NEMO PISC-ARAG	Observation-based estimates
Source							
Net $CaCO_3$ production	1.05	1.00	1.00	0.99	0.79	0.87	0.8–1.6[1,2,3,4,5]
Sinks							
Pelagic $CaCO_3$ dissolution	0.40	0.40	0.61	0.60	0.48	0.55	0.5 ± 0.2[6],
(% of tot. $CaCO_3$ production)	(38.1%)	(40.0%)	(61.0%)	(60.6%)	(60.8%)	(63.2%)	1.0 ± 0.5[4] (> 1500 m)
$CaCO_3$ flux at lower boundary	0.65	0.60	0.39	0.39	0.31	0.32	–
$CaCO_3$ burial flux	–	–	–	–	–	–	0.3
Related fluxes							
Export flux 100 m	0.80	0.76	0.81	0.83	0.60	0.63	0.6[7], 0.6–1.6[4]
(% of tot. $CaCO_3$ production)	(76.2%)	(76.3%)	(81.0%)	(83.8%)	(75.9%)	(72.4%)	–
Pelagic $CaCO_3$ dissolution 0–1 km, % of tot. production	0.036%	0.036%	26.0%	26.4%	2.5%	14%	60–80%[8]
Pelagic $CaCO_3$ dissolution 0–2 km, % of tot. dissolution	44%	52.3%	71.6%	71.3%	38%	58%	≥ 60%[6]

[1] Iglesias-Rodriguez et al. (2002b), [2] Lee (2001), [3] Jin et al. (2006), [4] Berelson et al. (2007), [5] Balch et al. (2007), [6] Feely et al. (2004), [7] Sarmiento et al. (2002), [8] Milliman and Droxler (1996).

BGD
7, 7029–7090, 2010

Table 3. Sensitivity of $CaCO_3$ production and of the CO_2-$CaCO_3$ production/dissolution feedback to different parameterizations and emission pathways. Emissions follow the High, Medium and Low scenario over the 21st century and are set to zero after 2100. The values are averaged over a 10-year period. N = not applicable.

	$CaCO_3$ prod., 1766 ($Pg\,C\,yr^{-1}$)	$CaCO_3$ prod., 1766–2100 (%)	$CaCO_3$ prod., 1766–2500 (%)	Feedback by 2100 (ppm)	Feedback by 2500 (ppm)
Sensitivity to parameterizations (High scenario)					
CALLIN1, calcite	1.06	−66	−42	−11.37	−24.32
CALLIN2, calcite	1.05	−22	−15	−3.60	−8.70
CALMIC1, calcite	1.06	−34	−16	−4.29	−10.85
CALMIC2, calcite	1.01	−20	−08	−2.53	−5.05
CALARAG, calcite	0.66	−32	−16	N	N
CALARAG, aragonite	0.32	−40	−25	N	N
CALARAG, total $CaCO_3$	0.98	−35	−19	−5.77	−6.81
CAL2ARAG, calcite by nanop.	0.34	−31	−15	N	N
CAL2ARAG, aragonite	0.32	−40	−25	N	N
CAL2ARAG, calcite by mesop.	0.30	−21	−14	N	N
CAL2ARAG, total $CaCO_3$	0.96	−31	−18	−5.78	−5.96
Sensitivity to scenarios					
CALARAG, tot. $CaCO_3$, High	0.98	−35	−19	−5.77	−6.81
CALARAG, tot. $CaCO_3$, Medium	0.98	−23	−11	−4.07	−5.01
CALARAG, tot. $CaCO_3$, Low	0.98	−5	−2	−1.26	−0.77

BGD
7, 7029–7090, 2010

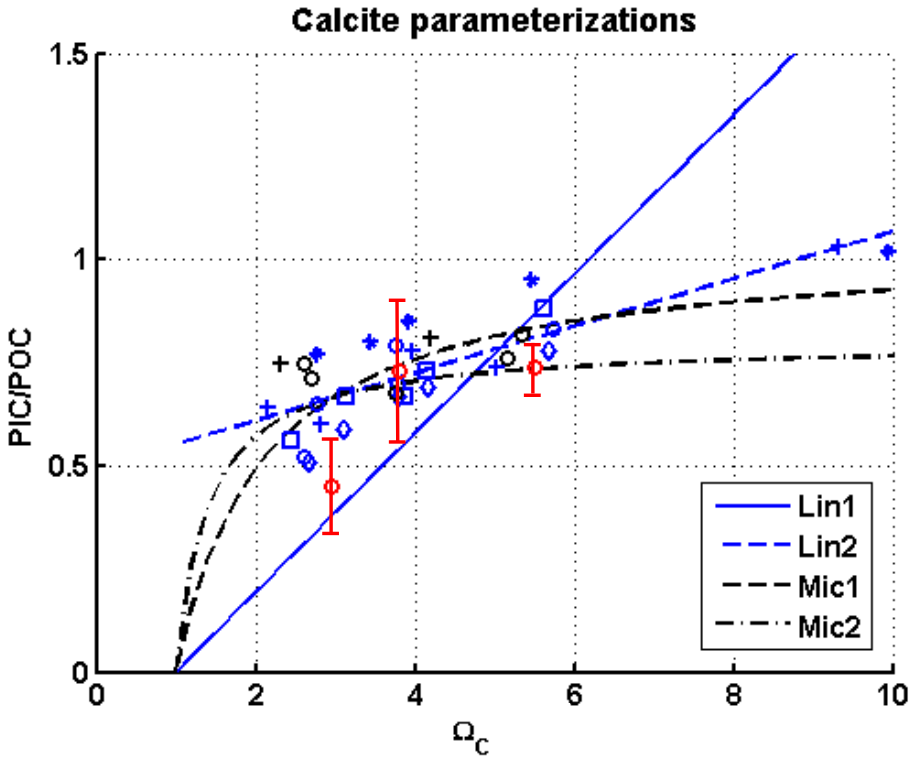

Fig. 1. PIC-POC ratio of calcifying nanophytoplankton as a function of calcite saturation state with respect to ambient waters. Data from Delille et al. (2005) is shown as red circles, 5 different studies from Zondervan et al. (2002) are shown as various blue symbols, data from Iglesias-Rodriguez et al. (2008) are shown as black circles and data from Shi et al. (2009) as black crosses. Three new parameterizations are fitted to the data and used in the Bern3D/PISCES model to compute $CaCO_3$ production: A Michaelis-Menten curve (MIC1), a linear curve that is forced to go through $\Omega_C = 1$ (LIN1) and a linear curve that was freely fitted to the data (LIN2). In addition, the Michaelis-Menten curve that was used in Gehlen et al. (2007) and Gangstø et al. (2008) is included (MIC2).

BGD
7, 7029–7090, 2010

Sensitivity of the marine carbonate cycle to atmospheric CO_2

R. Gangstø et al.

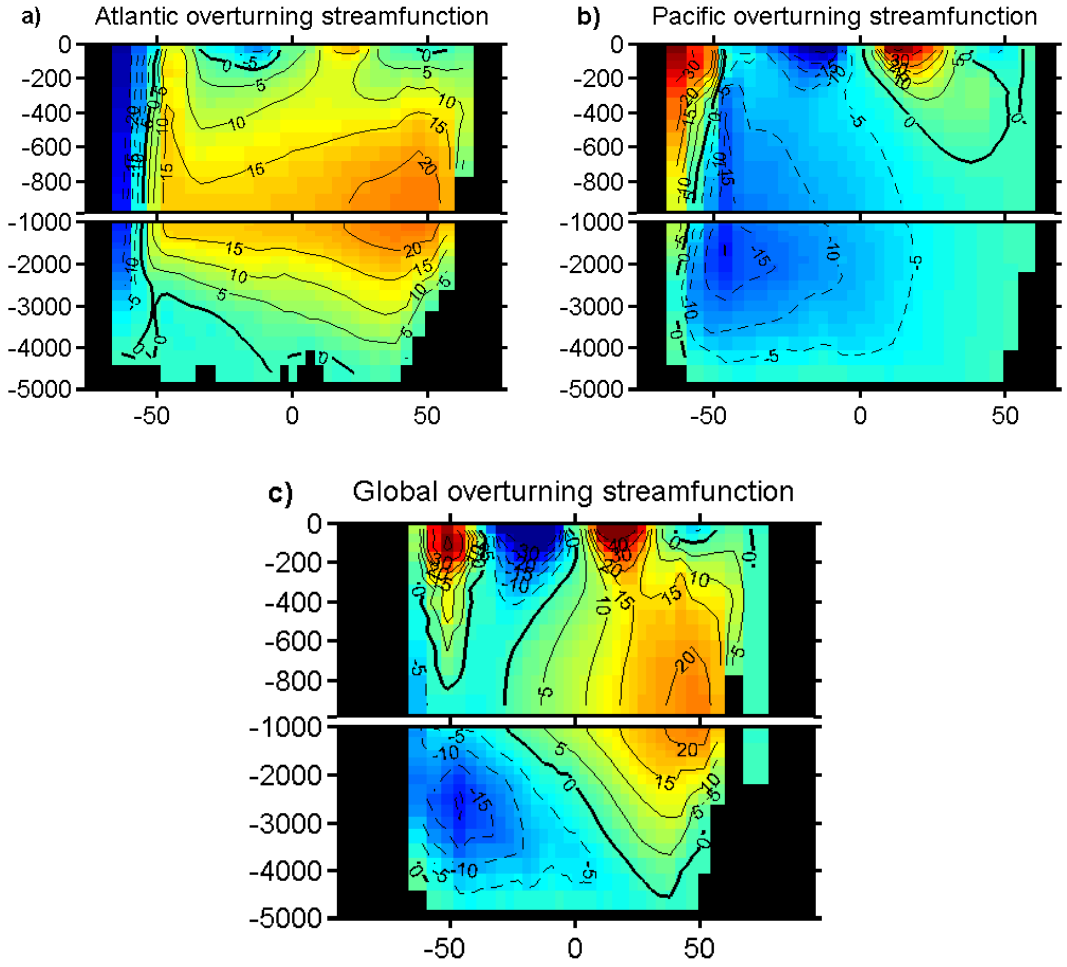

Fig. 2. Streamfunction of the Bern3D/PISCES model for the **(a)** Atlantic, **(b)** Pacific and **(c)** global ocean.

BGD
7, 7029–7090, 2010

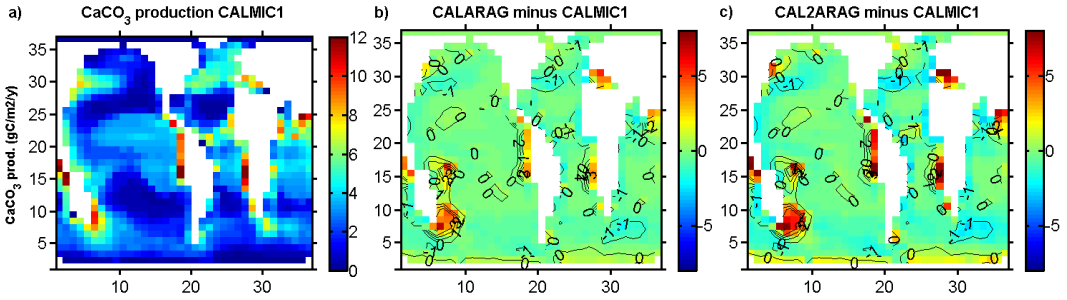

Fig. 3. Vertically integrated $CaCO_3$ production for **(a)** the version CALMIC1 that represents calcite production by nanophytoplankton only, **(b)** the difference to version CALARAG that represents calcite and aragonite production and **(c)** the difference to CAL2ARAG that represents calcite production by nano- and mesozooplankton and aragonite production.

BGD
7, 7029–7090, 2010

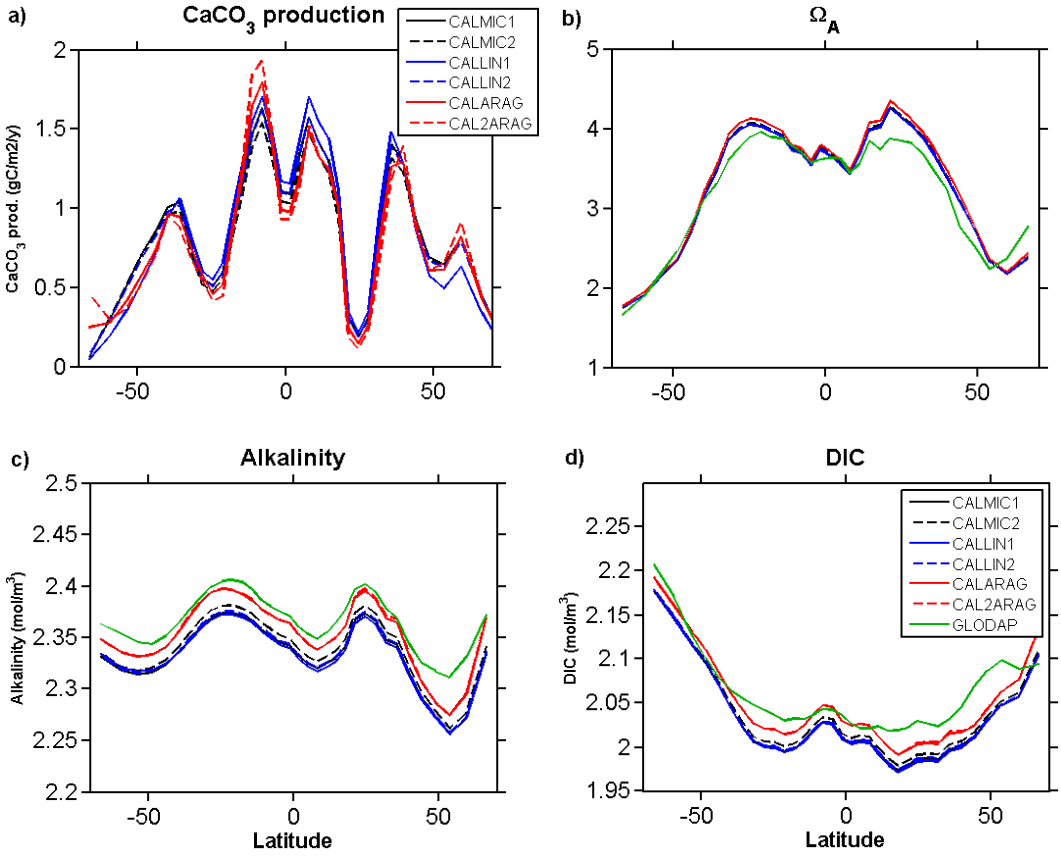

Fig. 4. Zonally-averaged **(a)** $CaCO_3$ production, **(b)** aragonite saturation state, **(c)** alkalinity and **(d)** DIC for the global ocean and different parameterizations of $CaCO_3$ production in the Bern3D/PISCES model. Observation-based estimates are shown by green lines (GLODAP; Key et al., 2004). All concentrations are averages over the upper 3 layers of the model, equivalent to a depth of 126 m.

BGD
7, 7029–7090, 2010

Sensitivity of the marine carbonate cycle to atmospheric CO_2

R. Gangstø et al.

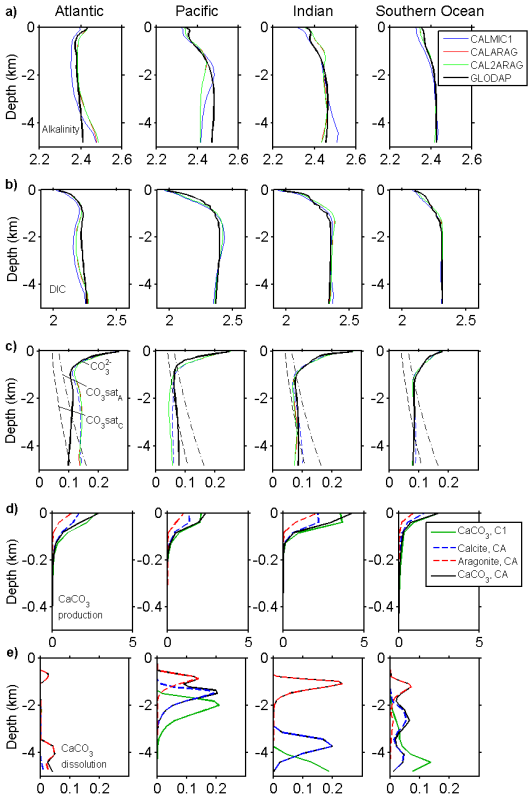

Fig. 5. Depth profiles for **(a)** alkalinity (mol m^{-3}), **(b)** DIC (mol m^{-3}), **(c)** CO_3^{2-} (mol m^{-3}), **(d)** $CaCO_3$ production (µmol kg^{-1} yr^{-1}) and **(e)** open water $CaCO_3$ dissolution (µmol kg^{-1} yr^{-1}). Concentrations (top rows) are shown for the Bern3D/PISCES versions CALMIC1, representing calcite production by nanophytoplankton only (blue), CALARAG, representing calcite and aragonite production (red) and CAL2ARAG, representing calcite production by nano- and mesozooplankton and aragonite production. Observation-based estimates are shown by black lines (GLODAP; Key et al., 2004) and saturation concentrations for CO_3^{2-} with respect to calcite and aragonite are indicated by grey, dashed lines. Production and dissolution (lower rows) of total $CaCO_3$ is shown for the versions CALMIC1 (green, C1) and CALARAG (black, CA); contributions by aragonite (dash, red) and calcite (dash, blue) are indicated for version CALARAG.

BGD
7, 7029–7090, 2010

Sensitivity of the marine carbonate cycle to atmospheric CO_2

R. Gangstø et al.

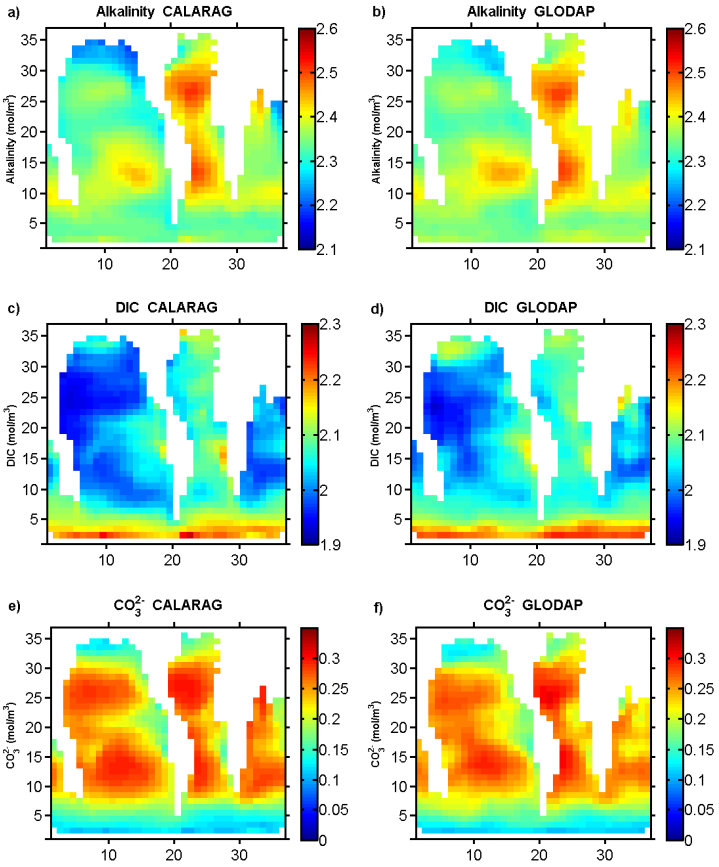

Fig. 6. Distribution of **(a, b)** alkalinity, **(c, d)** DIC and **(e, f)** carbonate ion concentrations simulated by the Bern3D/PISCES model (left) and from the GLODAP data (right; Key et al., 2004). Values are from the model version CALARAG that represents calcite and aragonite production and shown are averages over the top 3 layers of the model, equivalent to a depth of 126 m.

BGD
7, 7029–7090, 2010

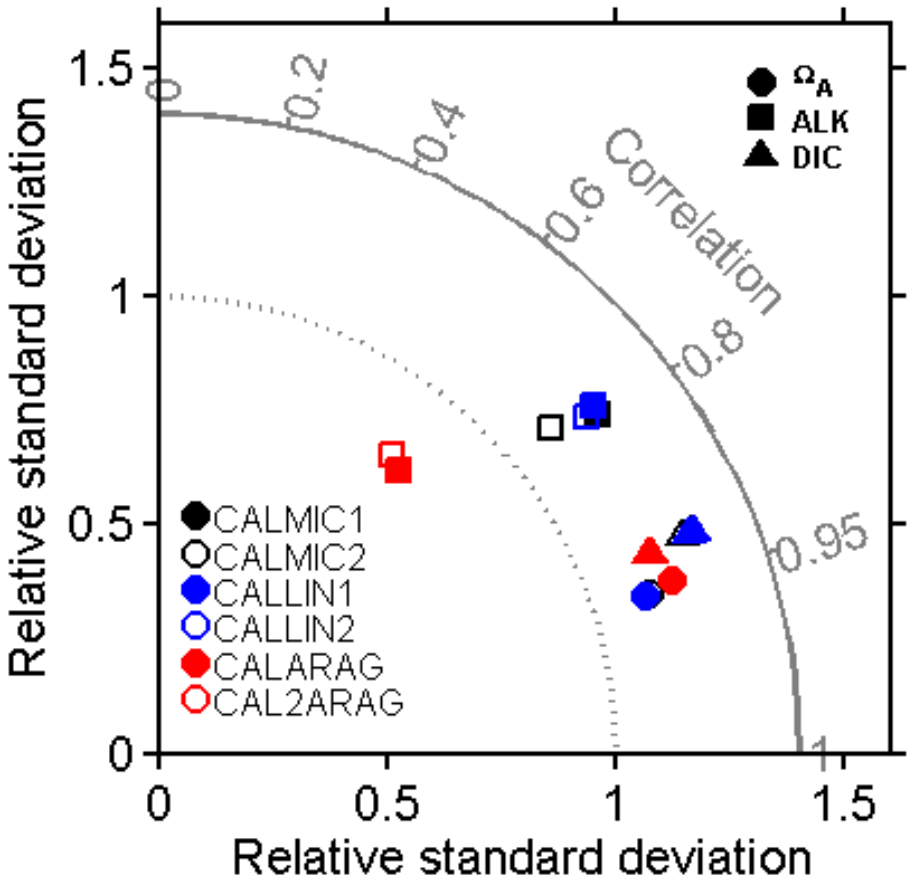

Fig. 7. Taylor diagram comparing modeled global fields of the saturation state with respect to aragonite, alkalinity, and DIC for different parameterizations of the $CaCO_3$ production to observation-based estimates (GLODAP; Key et al., 2004).

BGD
7, 7029–7090, 2010

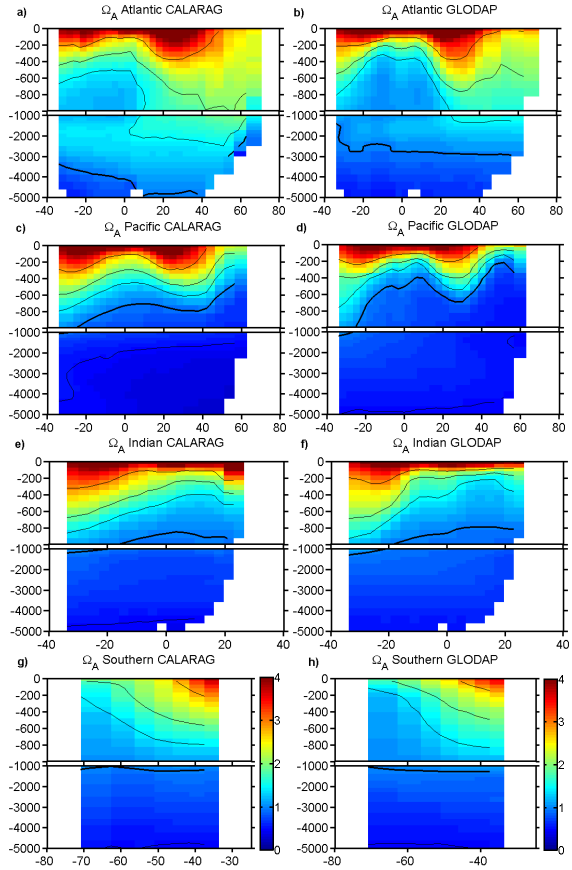

Fig. 8. Distribution of the aragonite saturation state simulated by the Bern3D/PISCES model (left; version CALMIC1) and based on observations from GLODAP (right). The saturation horizon in **(a)**, **(c)**, **(e)** and **(g)** is given for the $CaCO_3$ production parameterizations CALMIC1 (black, calcite only), CALARAG (grey, calcite and aragonite production) and CAL2ARAG (white, calcite by both nano- and mesozooplankton and aragonite). Values represent zonal averages.

BGD
7, 7029–7090, 2010

Sensitivity of the marine carbonate cycle to atmospheric CO_2

R. Gangstø et al.

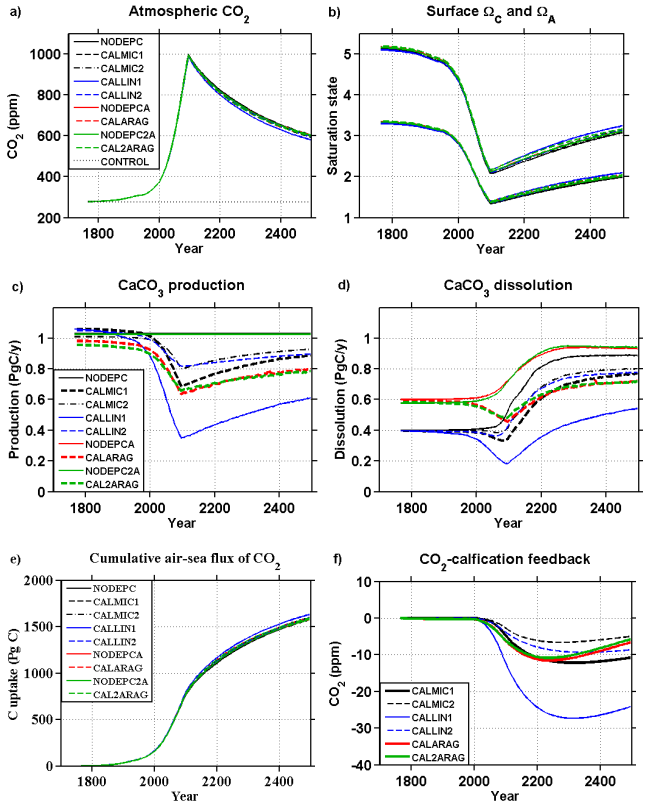

Fig. 9. Influence of different $CaCO_3$ production parameterizations for projected **(a)** atmospheric CO_2, **(b)** global-mean surface saturation states with respect to calcite and aragonite, **(c)** global $CaCO_3$ production, **(d)** global, open water $CaCO_3$ dissolution, **(e)** total cumulative air-sea flux of CO_2 and **(f)** the CO_2-$CaCO_3$ production/dissolution feedback quantified as the difference in atmospheric CO_2 between simulations with and without a dependency of $CaCO_3$ production on the saturation state. The Bern3D/PISCES model was forced with 21st carbon emissions from the high-emission scenario and emissions are hypothetically set to zero after 2100.

BGD
7, 7029–7090, 2010

Sensitivity of the marine carbonate cycle to atmospheric CO_2

R. Gangstø et al.

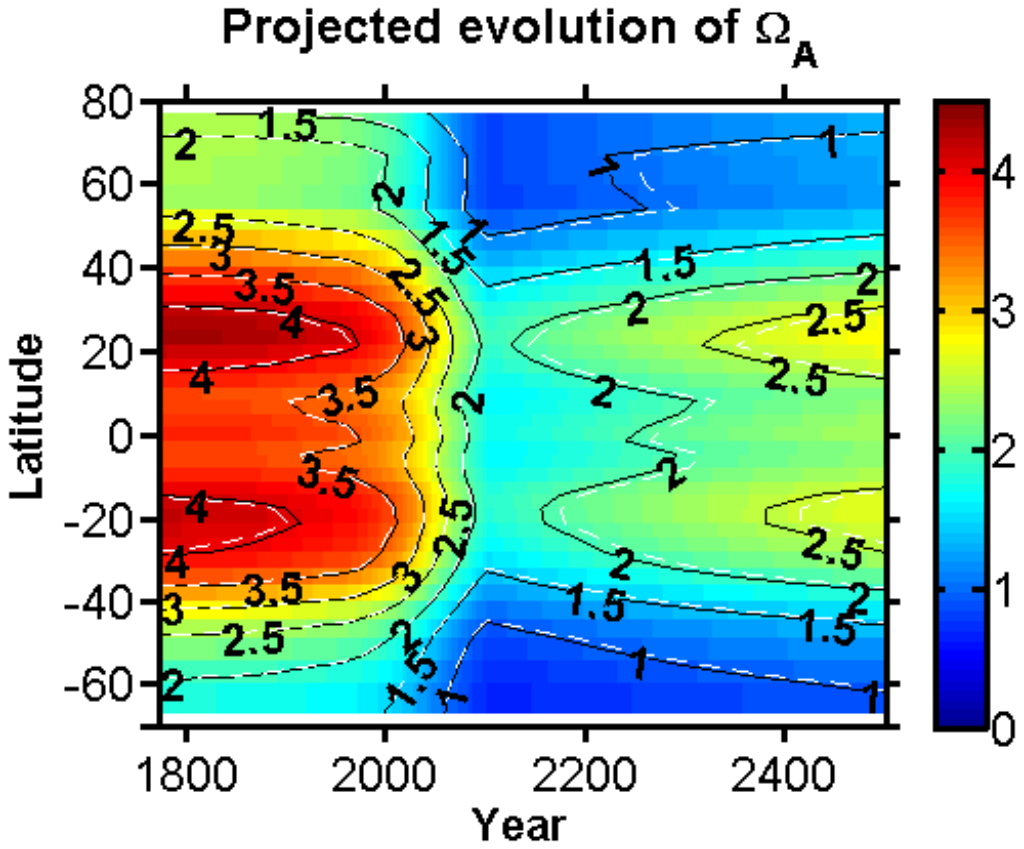

Fig. 10. Projected evolution of the aragonite saturation state in the surface ocean (top 125 m) for the High emission commitment scenario where carbon emissions increase in the 21st century following scenario RCP8.5. Color scale and black contour lines represent values from the CALARAG version that includes aragonite and calcite production. White contour lines are from the version with $CaCO_3$ production independent of the saturation state (NODEPCA).

BGD
7, 7029–7090, 2010

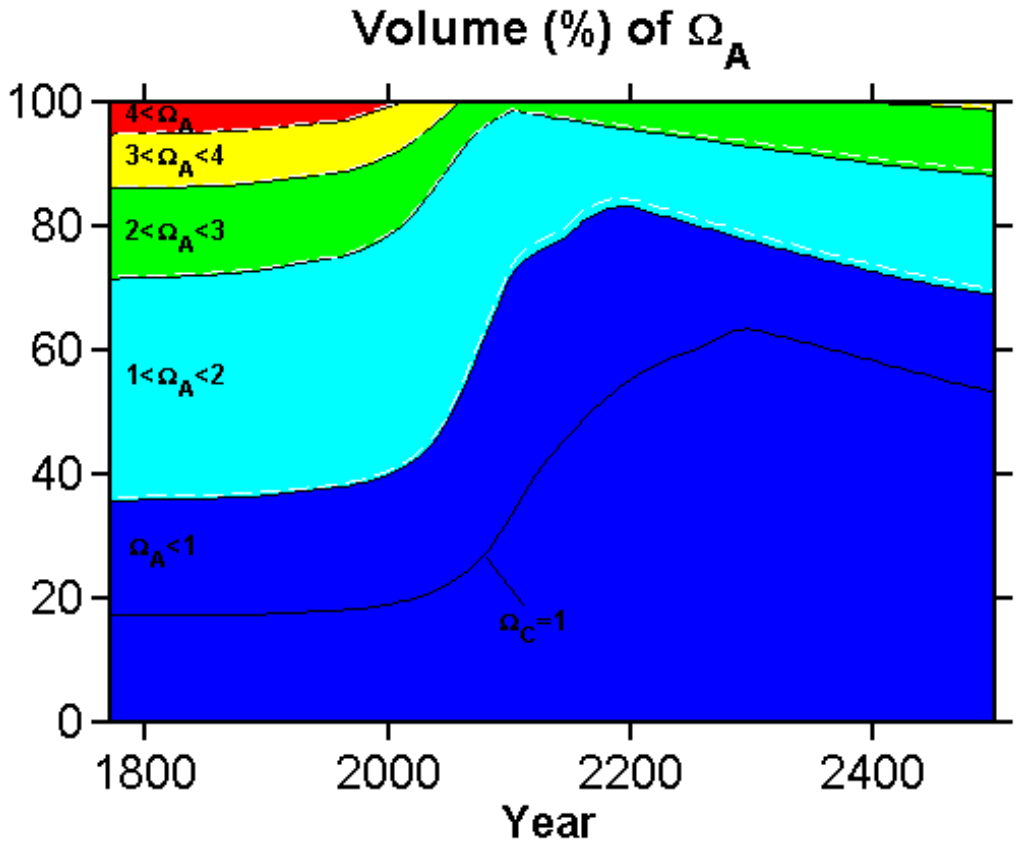

Fig. 11. Simulated global annual mean changes in the entire ocean volume of supersaturated (light blue to red) and undersaturated (blue) waters with respect to aragonite for the High emission commitment scenario where emissions are set to zero after 2100. Differences are small between the versions with (color, black contours,) and without (white contours) $CaCO_3$ production depending on saturation. The black dashed line indicates the separation between over and undersaturated water with respect to calcite.

BGD
7, 7029–7090, 2010

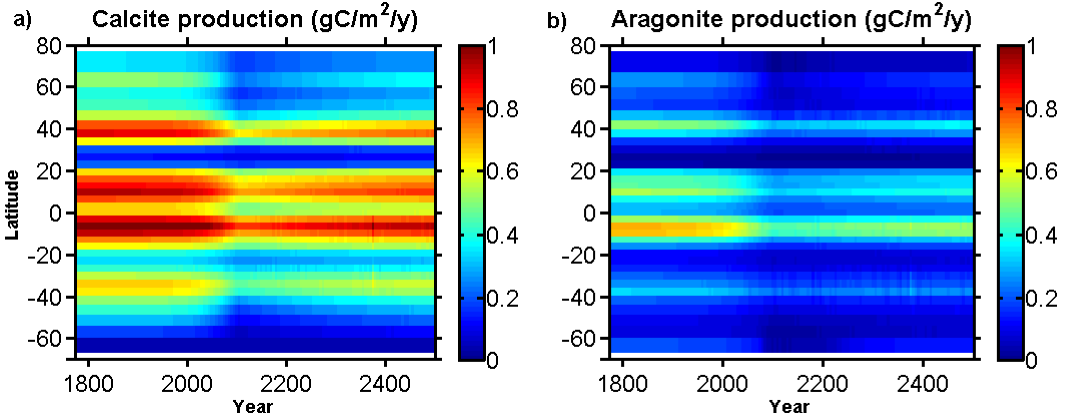

Fig. 12. Projected evolution of **(a)** calcite and **(b)** aragonite production ($g\,C\,m^{-2}\,yr^{-1}$) for the CALARAG version.

BGD
7, 7029–7090, 2010

Sensitivity of the marine carbonate cycle to atmospheric CO_2

R. Gangstø et al.

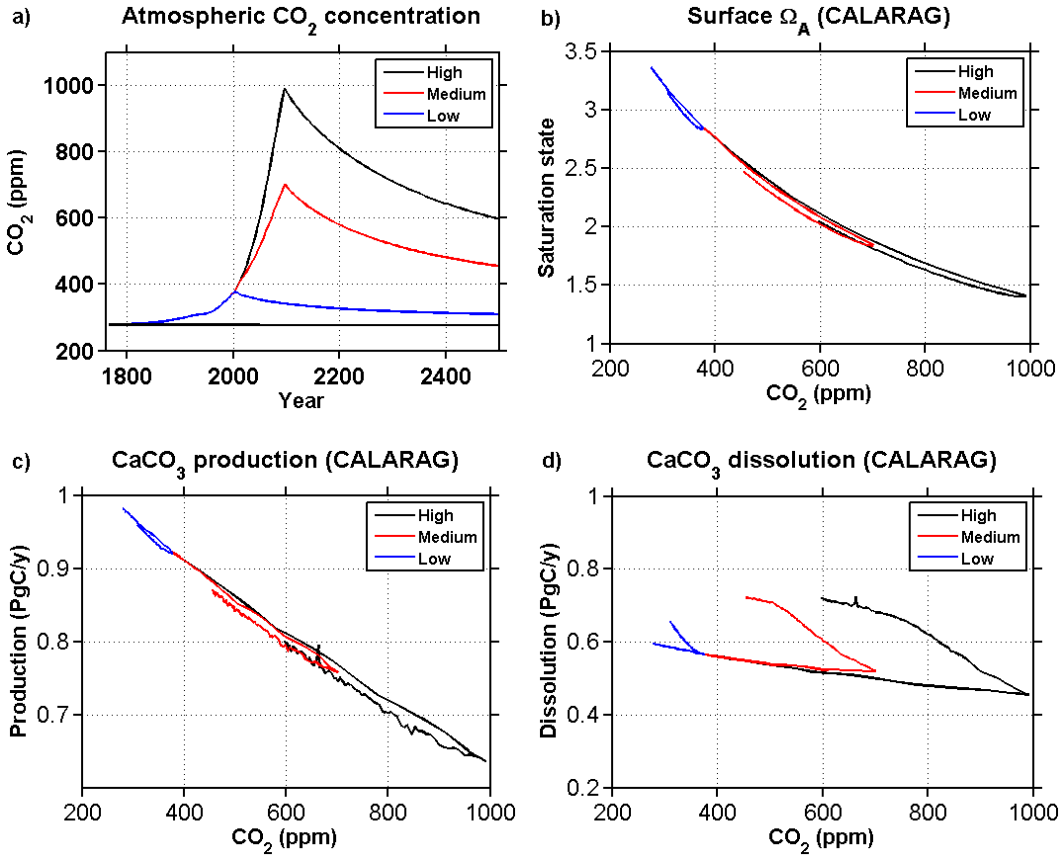

Fig. 13. Projected global mean values for a High, Medium, and Low emission scenario and for the Bern3D/PISCES version that includes aragonite and calcite production (CALARAG). Evolution of **(a)** atmospheric CO_2 as a function of time, **(b)** aragonite saturation state, **(c)** total $CaCO_3$ production, and **(d)** open water $CaCO_3$ dissolution as functions of atmospheric CO_2.

BGD
7, 7029–7090, 2010

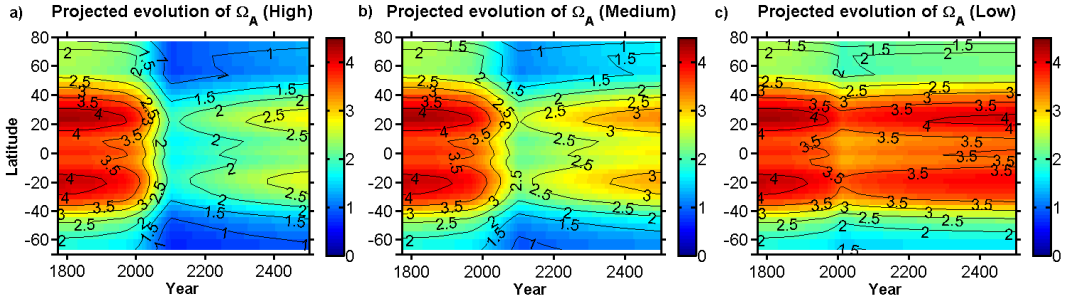

Fig. 14. Modeled evolution of zonal annual mean surface aragonite saturation state of the **(a)** High, **(b)** Medium and **(c)** Low emission commitment scenario and the CALARAG model version.

BGD
7, 7029–7090, 2010

Sensitivity of the marine carbonate cycle to atmospheric CO_2

R. Gangstø et al.